

# Mach-uniform accuracy and efficiency of a semi-implicit/explicit algorithm to solve compressible Euler equations for general fluids

Mikio Akamatsu<sup>a</sup>, Katsuhiro Watanabe<sup>b</sup> and Toshiyuki Arima<sup>c</sup>

**Abstract** This paper describes the feasibility of a novel finite-volume based Mach-uniform semi-implicit/explicit numerical framework, MUSE for brevity, to solve unsteady compressible flows of general fluids at arbitrary Mach numbers. For high-speed flows, an explicit temporal discretization with a high-resolution upwind scheme is used so as to accurately capture shock, contact and rarefaction waves. For low-speed flows, a semi-implicit discretization with a pressure-prediction-correction method is used in order to circumvent the time step restriction arising from the Courant-Freidrichs-Lewy (CFL) condition ; the high-resolution upwind scheme is used so as to preserve accuracy on the convective transport. These explicit and semi-implicit discretizations are integrated into a hybrid algorithm. In this paper, the E-CUSP scheme by G.-C. Zha is incorporated into the MUSE framework. To deal with general fluids, the GCUP method originated by K. Watanabe is introduced in a general form. Numerical experiments have been performed on a series of one-dimensional Riemann problems over a wide range of Mach numbers, from  $M=O(10^{-4})$  to supersonic, for a perfect gas and a liquid governed by the Tammann equation of state. The accuracy, efficiency and robustness of the proposed MUSE/E-CUSP\_GCUP are discussed, and we have confirmed the validity of the method at all speeds. Smooth transition between the semi-implicit and the explicit discretizations is demonstrated in the computation of a subsonic-supersonic flow transient due to a strong local heat generation.

**Key Words** CFD, FVM, compressible flow, Tammann EOS, stiffened gas EOS, Mach-uniform, all-speeds, E-CUSP, GCUP, MUSE, AUSM

**1. Introduction** The purpose of this study is to construct a Mach-uniform numerical method for solving unsteady compressible flows of general fluids. We will use the term ‘Mach-uniform’ to refer to the following properties of a numerical method :

- (I) when used for high-speed flows, shocks, rarefaction waves and contact discontinuities are captured at high-resolution,
- (II) for low-speed flows, the convective transport is accurately computed without the time step restriction arising from the Courant-Freidrichs-Lewy (CFL) stability condition.

There are two major approaches for constructing a method to solve compressible flow equations. The first one is density-based approach by which pressures are obtained through substituting densities into an equation of state. The flux difference splitting (FDS) and the flux vector splitting (FVS)

---

a CFD engineer

b Institute of Quantum Programming, Inc., 2-4-3-511 Cosmo Stage Wako, Chuo Wako-Shi Saitama, 351-0113 Japan, iqp.k-wata@jcom.home.ne.jp

c Honda R&D Co., Ltd., Fundamental Technology Research Center, 1-4-1 Chuo Wako-Shi Saitama, 351-0193 Japan, t.arima@f.rd.honda.co.jp

schemes[1] are the typical examples. These schemes have the above mentioned property (I), and are effective for high-speed flows. However, the following disadvantage may appear when applied to low-speed flows :

- (1) Density varies only weakly with pressure variation in low-speed flows, thus pressure solution computed from density tends to be inaccurate,
- (2) In the majority of practical computations on low-speed flows, the convective transport of mass, momentum and energy is of primary concern. Time scales of the transport phenomena are in general much larger than those of sound wave propagation in low-speed flows. If one uses an explicit temporal discretization, the time step,  $\Delta t$ , must be restricted by the CFL condition for stability :  $CFL_{\text{acos}} \leq \sigma$ , where  $CFL_{\text{acos}}$  is the *acoustic* CFL number defined as :

$$CFL_{\text{acos}} = \max_j ((|u_j| + c_j) \cdot \Delta t / \Delta x),$$

where  $u_j$  denotes the velocity at the grid point  $j$ ,  $c_j$  is the local sound speed,  $\Delta x$  is the grid spacing, and  $\sigma$  is a constant and generally less than unity. The acoustic CFL condition restricts the time step with the maximum propagation speed of the characteristic waves, which is much larger than the speed of convective transport, i.e., the velocity. Then, the CFL condition imposes excessive restriction on time step, which seriously deteriorates computational efficiency.

In order to circumvent the above issue (2), one can use an implicit discretization. However implicit methods generally tend to suffer from slow convergence due to large disparity among the eigenvalues of the system matrix under subsonic regime. To accelerate convergence, a technique using preconditioning of the system matrix combined with a pseudo-time steps has been developed[2-4]. The preconditioning techniques have been applied mainly to steady problems, and the efficiency against unsteady problems may not have been established. According to the review by Keshtiban et al.[5], finding suitable preconditioners with optimized properties for complex problems is far from straightforward.

The second one is pressure-based approach. Harlow and Amsden[6] presented their works along this approach in the context of all-speeds flow solver in around 1970, and have been followed by wide variety of schemes, including ICE[6], SIMPLE[7], CIP[8], WIMF[9], etc.. In low-speed flows, all these schemes circumvent the time step restriction imposed by the acoustic CFL condition by means of implicit treatment for the pressure. The SIMPLE advocates *fully implicit* discretization, so that the convection terms are also treated implicitly, and thus one can use large time step. However, implicit discretizations are generally more dissipative than explicit ones, and may seriously deteriorates solutions for unsteady flows. Hence, we do not take up a fully implicit discretization. In contrast, the ICE, CIP and WINF use a *semi-implicit* temporal discretization, where the convection terms are treated explicitly, while the pressure is treated implicitly. The present method partially adopts a semi-implicit discretization.

There are semi-implicit schemes[6,8-10] purporting to be ‘all-speeds’. These schemes satisfy the above-mentioned property (II), and they are efficient for low-speed flows. However, for high-speed flows, semi-implicit discretizations can not retain their advantage over explicit discretizations. Define the *convective* CFL number based on the fluid velocity as  $CFL_{\text{conv}} = \max_j (|u_j| \cdot \Delta t / \Delta x)$ . Semi-implicit discretizations treat convection terms explicitly, hence for the sake of stability, the *convective*

CFL condition expressed as  $CFL_{\text{conv}} \leq \tau$  must be satisfied, where  $\tau$  is a constant and generally less than unity. Assume that  $|u|$  and  $c$  attain the maximum values, for simplicity, at the same grid point  $j$ , when  $CFL_{\text{acos}}/CFL_{\text{conv}} = 1 + (1/M_j)$ . If the local Mach number  $M_j \ll 1$ , then  $CFL_{\text{acos}} \gg CFL_{\text{conv}}$ . Consequently, the time step determined by the convective CFL condition is much larger than that determined by acoustic CFL condition. Hence, semi-implicit discretizations retain efficiency at  $M_j \ll 1$ . In contrast, as  $M_j \uparrow 1$ , then  $CFL_{\text{acos}}/CFL_{\text{conv}} \downarrow 2$ , thus the efficiency of semi-implicit discretizations decreases. Semi-implicit discretizations generally require additional cost with iterative procedures to solve the pressure. Furthermore, the implicit part tends to produce excessive numerical dissipation which may impair the resolutions of shock and contact waves. Therefore, the advantage of semi-implicit discretizations disappears when  $M_j$  exceeds unity.

The above observation stimulates us to construct an alternative numerical framework based on a hybrid semi-implicit (for low speed)/explicit (for high speed) discretization, which we named MUSE for brevity representing Mach-uniform semi-implicit/explicit.

**2. Objectives and strategy** The objective of this paper is to draw a Mach-uniform numerical method to be used as a building block of a computer code for compressible multi-material flows. The goals are as follows :

1. To construct a finite-volume based Mach-uniform method for one-dimensional Euler equation. We particularly concentrate to make the algorithm be simple as much as possible so that we can pursue cumbersome multi-material model on a straightforward basic structure.
2. To implement a method to deal with general equation of state (EOS for brevity) for gases and liquids consistent with the temporal discretization.
3. To confirm accuracy, efficiency and robustness of the constructed method by numerical experiments.

We adopt the hybrid temporal discretization, in which we need to switch between semi-implicit/explicit discretization, for example, according to the maximum local Mach number within the computational domain. A lot of standard textbooks tell us that density change is assumed to become small when the Mach number is below 0.3, and low Mach number flows are usually considered to behave incompressibly. However, for instance, consider water hammer phenomenon, the compressibility of the liquid plays predominant roles, and high pressure waves or shocks are built up even if the Mach number is considerably small. Therefore, explicit temporal discretizations are recommended if one needs to capture those waves at high-resolution. Taking into account such circumstances, the MUSE framework allows to select both the explicit and the semi-implicit method according to the input parameter  $M_{\text{sw}}$  (the Mach number to switch semi-implicit/explicit) depending on one's demand for the level of resolution on shocks and rarefaction waves. Numerical experiments to be shown in §5.1 will provide information to decide which discretization is suited for the specific problem.

The hybrid discretization allows us to make use of the best suited method for each Mach number regimes, and provides flexibility for us to use both methods. In order to enhance this advantage, we have made an effort to integrate the semi-implicit and the explicit discretizations. As a result, the most part of the algorithm for the explicit discretization has been shared with the semi-implicit discretization

to be described in a later section. We construct the hybrid method along with the finite-volume approach in which the flux vector is split into the convective part and the acoustic (pressure) part. Such splitting is inconsistent with schemes which require an eigen-decomposition like the Roe's FDS[11]. Among a number of schemes to deal with the inviscid fluxes, we focused attention on the class of the CUSP (convective upwind and split pressure). The CUSP need not the eigen-decomposition, so that it is simple, although it is accurate to the same extent as the more rigorous Roe's FDS. Most importantly, the CUSP splits the flux vector into the convective part and the acoustic part. In this sense, the CUSP is consistent with our semi-implicit discretizations. Jameson[12] pointed out that the CUSP can be categorized to two types, the H-CUSP and E-CUSP. These schemes split the inviscid flux vector into convective terms and acoustic terms. The H-CUSP such as the Liou's AUSM[13] family has the total enthalpy, denoted by  $H$ , from the energy equation in their convective flux, while the E-CUSP has the total energy ( $E$ ). Zha and Hu[14] suggested that from the characteristic theory point of view, the H-CUSP are not fully consistent with the fluctuation propagation directions, which may affect the stability and robustness ; in contrast, the upwinding of the convective term and the pressure splitting of the E-CUSP are consistent with their characteristic directions. Accordingly, we employed the Zha E-CUSP[14-16] for the discretization of the flux in the present paper. Note that the H-CUSP including AUSM-family may also available within the present framework.

Most of the numerical methods for compressible flows intend to aerodynamic applications, so that they often assume the fluid to be governed by a perfect gas EOS. In contrast, we implement the GCUP originated by Watanabe[17] to deal with general fluids. As a rudimentary example, we consider the Tammann EOS[18] representing thermodynamic properties of liquids.

**3. Governing equations** The governing equations are the following compressible Euler equations in conservation law form in one space dimension :

$$\partial_t \mathbf{Q}(x, t) + \partial_x \mathbf{f}(\mathbf{Q}(x, t)) = \mathbf{0}, \quad (1)$$

where  $\mathbf{Q}$  is the vector of conserved variables :  $\mathbf{Q} = (\rho, \rho u, \rho E)^T$ ,  $\mathbf{f}$  is the flux vector :

$$\mathbf{f} = (\rho u, \rho u^2 + p, (\rho E + p)u)^T. \quad (2)$$

The quantities  $\rho, p, u$  and  $E$  respectively denote the pressure, density, velocity, total energy per unit mass ( $E = e + (1/2)u^2$  with  $e$  the internal energy per unit mass). In this paper, we limit our discussion within one-dimensional space, however we expect that the present method can be naturally extended to multi-dimension.

To deal with general fluids, we employ the following form of equation of state (EOS) which appears most frequently in literatures.

$$G(p, \rho, T) = 0. \quad (3)$$

where  $T$  is the temperature. To close the system of equations, we assume that we know a function to represent the enthalpy per unit mass,  $h = e + (p/\rho)$ , in terms of  $p, \rho, T$  :  $h = h(p, \rho, T)$ . Then we have the following equation :

$$\rho E - (\rho u^2 / 2) + p = \rho \cdot h(p, \rho, T). \quad (4)$$

The speed of sound, denoted by  $c$ , which plays important roles in compressible flows are represented as :

$$c = \sqrt{\left(\frac{\partial e}{\partial p}\right)^{-1} \left(\frac{p}{\rho} - \rho \left(\frac{\partial e}{\partial \rho}\right)\right)} / \rho. \quad (5)$$

The simplest example is the calorically perfect gas or polytropic ideal gas EOS, for which

$$G(p, \rho, T) = p - \rho(\gamma - 1) C_v T = 0, \quad (6)$$

$$h(p, \rho, T) = C_v T + (p/\rho), \quad (7)$$

$$c = \sqrt{\gamma p / \rho}, \quad (8)$$

where  $\gamma$  is the specific heat ratio ( $\gamma = C_p / C_v$ ), and  $C_v$  is the specific heat at constant volume ( $C_v = R / (\gamma - 1)$ ;  $R$  is the gas constant). In this paper,  $\gamma = 1.4$  and  $R = 1$  are taken in the numerical experiments to be described later.

Another EOS used in the present paper is the Tammann EOS[18] or ‘stiffened gas’ EOS which represents thermodynamic characteristics of liquids. This is formulated as :

$$G(p, \rho, T) = p - \rho(\gamma_c - 1) C_v T + \gamma_c p_0 = 0, \quad (9)$$

$$h(p, \rho, T) = C_v T + (p/\rho), \quad (10)$$

$$c = \sqrt{\gamma_c (p + p_0) / \rho}. \quad (11)$$

The constants,  $\gamma_c$  and  $p_0$ , are taken due to Gallouët, et al. as  $\gamma_c = 7.15$ ,  $p_0 = 3.0 \times 10^8$  to simulate water in the numerical experiments.

## 4. Numerical method

**4.1 Overall procedure** The algorithm of the present method can be conveniently written as follows :

- Given**  $M_{sw}$  ..... Mach number to switch semi-implicit/explicit discretization,  
 $\sigma_{max}$  ..... maximum allowable  $CFL_{acos}$  ; when the explicit discretization is used, the time step  $\Delta t$  is determined by
- $$\sigma_{max} = \max_j \left( |u_j| + c_j \right) \cdot \Delta t / \Delta x,$$
- $\tau_{max}$  ..... maximum allowable  $CFL_{conv}$  ; when the semi-implicit discretization is used, the time step  $\Delta t$  is determined by
- $$\tau_{max} = \max_j |u_j| \cdot \Delta t / \Delta x,$$
- id\_GCUP ... flag which indicates whether the GCUP is used.  
id\_GCUP= 1 ... used ; id\_GCUP= 0 ... not used.

## Solution Procedure

### 1) Select temporal discretization and time step

Starting from the cell-averages  $\{\mathbf{Q}_j^n\}$  at time  $t^n$ ,

- If  $\max_j M_j \geq M_{sw}$ , then ;

id\_switch  $\leftarrow$  'EX' : The *explicit* temporal discretization is selected, and the time step is determined as :

$$\Delta t = \sigma_{\max} \cdot \Delta x / \max_j \left( |u_j^n| + c_j^n \right) ;$$

Else then ;

id\_switch  $\leftarrow$  'SI' : The *semi-implicit* temporal discretization is selected, and the time step is determined as :

$$\Delta t = \tau_{\max} \cdot \Delta x / \max_j |u_j^n| .$$

### 2) Pressure prediction (only for semi-implicit discretization)

If id\_switch =SI ;

- Solve the momentum conservation only with the convective flux to yield the 'advanced' momentum  $(\rho u)_j^{\text{ad}}$  using a multi-stage Runge-Kutta time integration (§4.3, §4.4) ;
- From the cell-averages  $\{(\rho u)_j^{\text{ad}}\}$ , apply a non-oscillatory interpolation to yield the 'advanced' interface mass flux  $(\rho u)_{j+1/2}^{\text{ad}}$  (§4.2) ;
- Solve the pressure equation (Eq.(13)) using  $(\rho u)_{j+1/2}^{\text{ad}}$  to obtain the 'advanced' pressure  $\{p_j^{\text{ad}}\}$ .

### 3) Solve conservation law

- Solve the conservation laws (Eq.(1)) using the Runge-Kutta time integration to yield the predicted cell-average  $\{\mathbf{Q}_j^{n+1*}\} = \{(\rho_j^{n+1*}, (\rho u)_j^{n+1*}, (\rho E)_j^{n+1*})^T\}$  at the '(n+1)\*th' time step. ;

In each stage of the Runge-Kutta integration, compute the mass, momentum and energy flux by the Zha E-CUSP scheme (§4.4.1) with the MUSCL reconstruction ;

Treat the pressure in the following manner :

If id\_switch =EX and id\_GCUP=1, then ;

Fix the pressure as  $p = p^n$  through the Runge-Kutta integration ;

Else if id\_switch =SI, then ;

Fix the pressure as  $p = p^{\text{ad}}$  through the Runge-Kutta integration ;

If id\_switch =EX and id\_GCUP=0, then ;

Solve the EOS (Eq.(3)) with the enthalpy relation (Eq.(4)) substituting the temporal solution of the conservation law,  $\mathbf{Q}^{(m)} = (\rho^{(m)}, \rho u^{(m)}, \rho E^{(m)})^T$ , to yield the temporal pressure,  $p^{(m)}$ , in each stage of the Runge-Kutta time integration.

### 4) Update the cell-averages $\{\mathbf{Q}_j^{n+1*}\}$ at time $t^{n+1}$

If id\_GCUP=1, then ;

- Starting from  $\{\mathbf{Q}_j^{n+1*}\}$ , correct the pressure so that (n+1)th time-level state variables  $p^{n+1}$ ,  $\rho^{n+1}$  and  $T^{n+1}$  satisfy given EOS. Apply the GCUP iteration as follows until given convergence criteria are satisfied : (§4.5)

For  $m = 1, 2, 3, \dots$  ;

- Solve the pressure-correction equation (Eq.(43), (57), (58)) in an elliptic form to yield the pressure-correction,  $\delta p_j^{(m)}$  ;
- Compute the density, momentum and energy correction,  $\delta \rho_j^{(m)}$ ,  $\delta \rho u_j^{(m)}$ ,  $\delta \rho E_j^{(m)}$  from  $\delta p_j^{(m)}$  ;
- Compute the pressure and the cell-averaged conserved variables as ;

$$p_j^{(m)} = p_j^{(m-1)} + \delta p_j^{(m)}, \quad \mathbf{Q}_j^{(m)} = \mathbf{Q}_j^{(m-1)} + \delta \mathbf{Q}_j^{(m)} ;$$

- After achieving convergence, update the pressure and the conserved variables :

$$p_j^{n+1} = p_j^{(m)}, \quad \mathbf{Q}_j^{n+1} = \mathbf{Q}_j^{(m)} ;$$

Else if  $\text{id\_GCUP}=0$ , then ;

- Update the cell-averaged conserved variables as :

$$\mathbf{Q}_j^{n+1} \leftarrow \mathbf{Q}_j^{n+1*} ;$$

- If  $\text{id\_switch}=\text{SI}$ , then ;

Solve the EOS (Eq.(3)) with the enthalpy relation (Eq.(4)) substituting  $\mathbf{Q}^{n+1}$  to yield the new pressure  $p^{n+1}$ .

**4.2 Pressure prediction** The semi-implicit discretization treats the acoustic part of the flux in an implicit fashion (see Eq.(42)), so that at low Mach numbers, the CFL stability condition can be avoided. The pressure at time  $t^{n+1}$  is firstly predicted by solving the following Poisson-type linear pressure equation :

$$(p_j - p_j^n) / \Delta t = \Delta t (c_j^n)^2 \partial^2 p / \partial x^2 \Big|_j - (c_j^n)^2 \partial (\rho u)^{\text{ad}} / \partial x \Big|_j, \quad (12)$$

, where  $(\rho u)^{\text{ad}}$  is the ‘advanced’ momentum described below, which is the solution of the momentum convection equation in conservation form,  $\partial_t \rho u + \partial_x \rho u^2 = 0$ . See appendix for the derivation of Eq.(12).

Eq.(12) is discretized in each grid-cell as :

$$p_j = (c_j^n)^2 (\Delta t^2 / \Delta x^2) (p_{j+1} - 2p_j + p_{j-1}) - (c_j^n)^2 (\Delta t / \Delta x) \left\{ (\rho u)_{j+1/2}^{\text{ad}} - (\rho u)_{j-1/2}^{\text{ad}} \right\} + p_j^n, \quad (13)$$

$$j = 1, 2, 3, \dots, N_{\text{cell}} \quad (N_{\text{cell}} : \text{total number of grid cells}).$$

This linear system of equations is solved in terms of  $p$  using a tri-diagonal matrix solver in one space dimension, while using an iterative Krylov method such as CG and GMRES[19] in multi-dimensions. We term the solution ‘advanced’ pressure and denote by  $p^{\text{ad}}$ . In Eq.(13),  $\text{div}(\rho u)^{\text{ad}}$  is discretized in terms of the *cell-interface* mass flux,  $(\rho u)_{j+1/2}^{\text{ad}}$ , in order to enforce pressure-velocity coupling, which is particularly important for low-speed flows. In the following, we show how to obtain  $(\rho u)_{j+1/2}^{\text{ad}}$ .

At first, we solve  $\partial_t \rho u + \partial_x \rho u^2 = 0$  to obtain the *cell-averaged* ‘advanced’ momentum  $(\rho u)_j^{\text{ad}}$  using the Runge-Kutta time integration with the slope limiter described in §4.3 and §4.4. Next we reconstruct a piecewise-linear interpolant of  $(\rho u)^{\text{ad}}$  on grid-cells, which is then projected on its staggered cell-averages. We apply the non-oscillatory second-order projection algorithm used in the high-resolution central scheme by Nessyahu and Tadmor[20, 21]. Starting with initial data  $\{(\rho u)_j^{\text{ad}}\}$ , we re-

construct a piecewise-linear interpolant :

$$(\rho u)^{\text{ad}}(x) = \sum_j \left\{ \left[ (\rho u)_j^{\text{ad}} + d(\rho u)^{\text{ad}}/dx|_j \cdot (x - x_j)/\Delta x \right] \cdot \chi_j(x) \right\}, \quad (14)$$

where  $\chi_j(x)$  is the characteristic function of the grid-cell  $C_j$ ,

$$\chi_j(x) = \begin{cases} 1, & \text{if } x \in C_j; \\ 0, & \text{if } x \notin C_j. \end{cases} \quad \forall j,$$

and  $d(\rho u)^{\text{ad}}/dx$  is the limited discrete slope. Here we use the minmod- $\theta$ [20] limiter with  $\theta = 2$  :

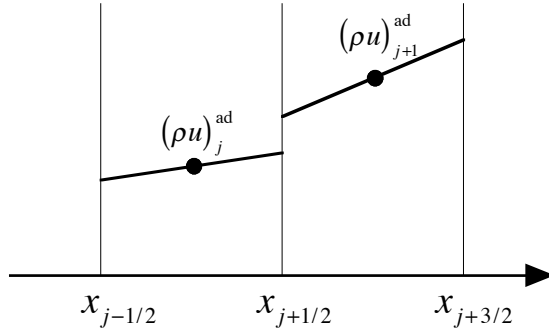
$$\begin{aligned} & \left( d(\rho u)^{\text{ad}}/dx \right) \Big|_j \\ & \approx \text{minmod} \left( \theta \left( (\rho u)_{j+1}^{\text{ad}} - (\rho u)_j^{\text{ad}} \right), \frac{1}{2} \left( (\rho u)_{j+1}^{\text{ad}} - (\rho u)_{j-1}^{\text{ad}} \right), \theta \left( (\rho u)_j^{\text{ad}} - (\rho u)_{j-1}^{\text{ad}} \right) \right). \end{aligned} \quad (15)$$

The minmod function are defined as :

$$\text{minmod} \left( x_1, x_2, \dots \right) = \begin{cases} \min_k \{ x_k \} & \text{if } x_k > 0 \text{ for all } k, \\ \max_k \{ x_k \} & \text{if } x_k < 0 \text{ for all } k, \\ 0 & \text{otherwise.} \end{cases} \quad (16)$$

The interpolant Eq.(14) is projected on the *staggered-cell average*  $(\rho u)_{j+1/2}^{\text{ad}}$ . Consequently,

$$(\rho u)_{j+1/2}^{\text{ad}} = \frac{1}{2} \left\{ (\rho u)_j^{\text{ad}} + (\rho u)_{j+1}^{\text{ad}} \right\} + \frac{1}{8} \left\{ d(\rho u)^{\text{ad}}/dx|_j - d(\rho u)^{\text{ad}}/dx|_{j+1} \right\}. \quad (17)$$



### 4.3 Temporal discretization

For the time integration of the conservation law, we employ the three-stage Runge-Kutta (RK) scheme due to Shu and Osher[22,1] which is known as TVD (Total variation Diminishing) RK or SSP (Strong Stability Preserving) RK scheme.

Consider the initial value problem,

$$d\mathbf{Q}_j(t)/dt = \mathcal{L}(\mathbf{Q}(t); j), \quad \mathbf{Q}_j(t^n) = \mathbf{Q}_j^n, \quad (18)$$

$$\mathcal{L}(\mathbf{Q}(t); j) \triangleq - \left( \mathbf{F}_{j+1/2}(t) - \mathbf{F}_{j-1/2}(t) \right) / \Delta x,$$

where  $\mathbf{F}_{j+1/2}(t)$  and  $\mathbf{F}_{j-1/2}(t)$  are cell-interface numerical fluxes, to be described in §4.4, at time  $t$ . Using third-stage TVD RK, the solution at the  $(n+1)$ \*th time step  $\{\mathbf{Q}_j^{n+1*}\}$  can be written as :

$$\mathbf{Q}_j^* = \mathbf{Q}_j^n + \Delta t \mathcal{L}(\mathbf{Q}^n; j), \quad (19a)$$

$$\mathbf{Q}_j^{**} = (3/4) \mathbf{Q}_j^n + (1/4) \mathbf{Q}_j^* + (1/4) \Delta t \mathcal{L}(\mathbf{Q}^*; j), \quad (19b)$$

$$\mathbf{Q}_j^{n+1*} = (1/3) \mathbf{Q}_j^n + (2/3) \mathbf{Q}_j^{**} + (2/3) \Delta t \mathcal{L}(\mathbf{Q}^{**}; j). \quad (19c)$$

**4.4 Discretization of flux** The discretization of the inviscid flux terms in this paper is based on the Zha E-CUSP scheme by Zha and Hu[14]. For a calorically perfect gas EOS, the inviscid flux  $\mathbf{f}$  has a homogeneous function of degree one in  $\mathbf{Q}$ , and it follows that  $\mathbf{f} = (\partial \mathbf{f} / \partial \mathbf{Q}) \cdot \mathbf{Q}$  [1]. The flux Jacobi matrix  $\mathbf{A} = (\partial \mathbf{f} / \partial \mathbf{Q})$  is diagonalizable, and the following representation is possible[14] :

$$\mathbf{f} = \mathbf{A}\mathbf{Q} = \mathbf{R} \begin{pmatrix} u & 0 & 0 \\ 0 & u & 0 \\ 0 & 0 & u \end{pmatrix} \mathbf{R}^{-1} \mathbf{Q} + \mathbf{R} \begin{pmatrix} -c & 0 & 0 \\ 0 & 0 & 0 \\ 0 & 0 & c \end{pmatrix} \mathbf{R}^{-1} \mathbf{Q}, \quad (20)$$

$$\mathbf{R} = \begin{pmatrix} 1 & 1 & 1 \\ u-c & u & u+c \\ H-uc & (1/2)u^2 & H+uc \end{pmatrix},$$

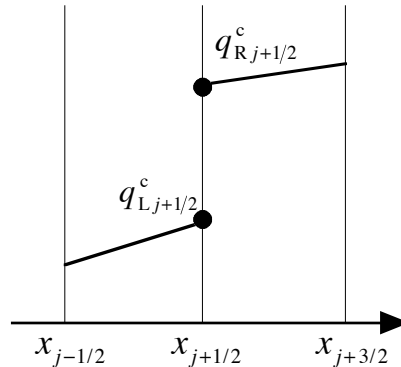
where  $c$  is the local speed of sound,  $H$  is the total enthalpy per unit mass, and  $\mathbf{R}$  is the right eigenvector matrix. It is easy to see that Eq.(20) can be rewritten as :

$$\mathbf{f} = \mathbf{f}^c + \mathbf{f}^p, \quad \mathbf{f}^c = u\mathbf{Q} = (\rho u, \rho u u, \rho u E)^T, \quad \mathbf{f}^p = (0, p, pu)^T. \quad (21)$$

In the right-hand side of Eq.(20), the inviscid flux  $\mathbf{f}$  consists of two parts. The first part provides the propagation of the fluctuations,  $\mathbf{l}_k \cdot d\mathbf{Q}$  ( $\mathbf{l}_k$  is the  $k$ -th row vector of  $\mathbf{R}^{-1}$  or the  $k$ -th left eigenvector ;  $k = 1, 2, 3$ ), along the flow path-line at the flow velocity  $u$ . The second part provides the propagation of the fluctuations in both upwind and downwind directions at the sound speed  $c$ . Accordingly, the vector  $\mathbf{f}^c$  represents the ‘convective part’ of the flux, while  $\mathbf{f}^p$  represents the acoustic part. This observation leads to the E-CUSP scheme that has the total energy term in the convective vector  $\mathbf{f}^c$ .

**4.4.1 Convective flux terms** Zha E-CUSP scheme discretizes the convective part of the flux vector at a cell-interface in the standard ‘upwind’ fashion as :

$$\mathbf{F}_{j+1/2}^c = (1/2) \left\{ (\rho u)_{j+1/2} \left( \mathbf{q}_{Lj+1/2}^c + \mathbf{q}_{Rj+1/2}^c \right) - |\rho u|_{j+1/2} \left( \mathbf{q}_{Rj+1/2}^c - \mathbf{q}_{Lj+1/2}^c \right) \right\}, \quad (22)$$



where  $\mathbf{F}$  denotes numerical flux, and  $(\rho u)_{j+1/2}$  is the cell-interface mass flux, the vector  $\mathbf{q}^c$  is

$$\mathbf{q}^c = (1, u, E)^T, \quad (23)$$

and the suffix ‘L’ and ‘R’ denote the states at the left and right sides of the cell-interface, respectively. The left and right states of  $u$  is evaluated using the van Leer MUSCL[23] reconstruction with the  $\beta$ -minmod slope limiter developed by Chakravarthy and Osher[24, 25] as follows :

For  $q = u$ ,

$$q_{L,j+1/2} = q_j + (1/4) \left\{ (1 - \kappa) \cdot \Delta^+ q_{j-1/2} + (1 + \kappa) \cdot \Delta^+ q_{j+1/2} \right\},$$

$$\Delta^+ q_{j-1/2} = \min \text{mod} \left( q_j - q_{j-1}, \beta (q_{j+1} - q_j) \right), \quad (24a)$$

$$\Delta^+ q_{j+1/2} = \min \text{mod} \left( q_{j+1} - q_j, \beta (q_j - q_{j-1}) \right),$$

$$q_{R,j+1/2} = q_{j+1} - (1/4) \left\{ (1 - \kappa) \cdot \Delta^- q_{j+3/2} + (1 + \kappa) \cdot \Delta^- q_{j+1/2} \right\},$$

$$\Delta^- q_{j+3/2} = \min \text{mod} \left( q_{j+2} - q_{j+1}, \beta (q_{j+1} - q_j) \right), \quad (24b)$$

$$\Delta^- q_{j+1/2} = \min \text{mod} \left( q_{j+1} - q_j, \beta (q_{j+2} - q_{j+1}) \right).$$

We use the above scheme generally under  $\kappa = 1/3$  corresponding to the highest formal accuracy, i.e., third-order, and the crispest setup of the compression parameter, i.e.,  $\beta = 4$  (the maximum value for preserving TVD for linear advections).

As for the reconstruction of the total energy per unit mass  $E$ , we take the following componentwise approach according to our numerical experiments :

- Apply the MUSCL reconstruction Eq.(24) for  $q = \rho e$  and  $q = \rho$  to yield  $(\rho e)_{L/R,j+1/2}$  and  $\rho_{L/R,j+1/2}$ .
- Then reconstruct  $E$  as the sum of the internal energy and the kinetic energy per unit mass:

$$E_{L/R,j+1/2} = (\rho e)_{L/R,j+1/2} / \rho_{L/R,j+1/2} + (1/2)(u_{L/R,j+1/2})^2.$$

When we took direct reconstruction of  $E$  using Eq.(24) for a supersonic liquid flow (case15 to be shown in §5.1), the solution suffered from a negative pressure near the origin ( $x \approx 0$ ) at the initial stage of the computation. In this case, the velocity  $u$  took a local peak near the point in the issue, whereas  $E$  was monotone. Then the direct interpolation of  $E$  could not reflect the drastic local change of the kinetic energy, and consequently severe undershoot occurred in the total energy ; here, notice that the kinetic energy may predominant over the internal energy in high speed flow regime. The componentwise approach is robust under these circumstances.

To construct the convective flux term, Zha borrowed the method to evaluate the cell-interface mass flux from the AUSMD scheme developed by Wada and Liou[26]. The method evaluates the cell-interface mass flux denoted by  $(\rho u)_{1/2}$  as follows:

$$(\rho u)_{1/2} = \rho_L u_L^+ + \rho_R u_R^-, \quad (25)$$

where the density  $\rho_L$  and  $\rho_R$  have been evaluated above using the MUSCL reconstruction. The cell-edge velocities are determined as follows :

$$u_L^+ = \begin{cases} \alpha_L \left\{ (u_L + c_m)^2 / (4c_m) - (u_L + |u_L|) / 2 \right\} + (u_L + |u_L|) / 2, & \text{if } |u_L| < c_m, \\ (u_L + |u_L|) / 2, & \text{otherwise,} \end{cases} \quad (26)$$

$$u_R^- = \begin{cases} \alpha_R \left\{ -(u_R - c_m)^2 / (4c_m) - (u_R - |u_R|) / 2 \right\} + (u_R - |u_R|) / 2, & \text{if } |u_R| < c_m, \\ (u_R - |u_R|) / 2, & \text{otherwise,} \end{cases} \quad (27)$$

$$\text{where } c_m = \max(c_L, c_R), \quad (28)$$

$$\alpha_L = 2\bar{\alpha}_L / (\bar{\alpha}_L + \bar{\alpha}_R), \quad \alpha_R = 2\bar{\alpha}_R / (\bar{\alpha}_L + \bar{\alpha}_R), \quad (29)$$

$$\bar{\alpha}_L = f(p_L, p_R) / (\rho_L c_m), \quad \bar{\alpha}_R = f(p_R, p_L) / (\rho_R c_m). \quad (30)$$

In the above formulation, cell-edge sound speeds,  $c_L$  and  $c_R$ , are evaluated by the left and right states of the pressure and density. The pressure  $p_L$  and  $p_R$  are again evaluated by the MUSCL reconstruction with the  $\beta$ -minmod limiter defined as Eq.(24) when the explicit discretization is used (id\_switch =EX). On the other hand, when the semi-implicit discretization is used (id\_switch =SI), we introduce a common interface pressure :  $p_{Lj+1/2} = p_{Rj+1/2} = (p_j + p_{j+1}) / 2$ .

**Remark** We employed Eq.(28) by Wada and Liou[26] for the common interface speed of sound,  $c_m$ . Zha and Hu[14] differently determined this quantity as  $c_m = (1/2)(c_L + c_R)$ .

In Eq.(30),  $f$  is some function of  $p_L$  and  $p_R$ . Wada and Liou took, according to their numerical experiments,

$$f(p_L, p_R) = p_L, \quad f(p_R, p_L) = p_R. \quad (31)$$

Consider stationary or moving contact discontinuity. It is known that the pressure and the velocity are constant around a contact discontinuity, thus  $p_L = p_R$  and  $u_L = u_R$ . Put  $u_{1/2} \triangleq u_L = u_R$ , then,

$$\alpha_L = 2\rho_R / (\rho_L + \rho_R), \quad \alpha_R = 2\rho_L / (\rho_L + \rho_R). \quad (32)$$

Rearrangement of Eq.(32) and Eqs.(25)-(27) leads to a mass flux formula :

$$(\rho u)_{1/2} = (1/2) u_{1/2} (\rho_L + \rho_R) - (1/2) |u_{1/2}| (\rho_R - \rho_L),$$

which is consistent with the exact solution of the Riemann problem. The AUSMD has this favorable property.

Wada and Liou[26] suggest that an arbitrary function might be possible as  $f$ . Our experiences indicate that the AUSMD under the above choice for  $f$  works well for the calorically perfect gas, however, the choice may result in negative pressure for liquids governed by the Tammann EOS. One of the remedy for this issue that we have firstly attempted is to modify Eq.(31) as :

$$f(p_L, p_R) = p_L + p_0, \quad f(p_R, p_L) = p_R + p_0. \quad (33)$$

We have confirmed this choice is a nice cure. However, Eq.(33) can not be applied for general EOS. Thus, we take the following setup as a present measure :

$$f(p_L, p_R) = f(p_L, p_R) \equiv \text{constant} (\neq 0), \text{ for liquids.} \quad (34)$$

With this choice, we have obtained satisfactory solutions for numerical experiments to be described in section 5.1.

**Remark** *This modification is not necessary when the semi-implicit method is used, since then the common interface pressure is taken :  $p_{Lj+1/2} = p_{Rj+1/2} = (p_j + p_{j+1})/2$  as already noted.*

Zha[15] have proposed a modified version, ‘Zha CUSP2’, in which  $\bar{\alpha}_L$  and  $\bar{\alpha}_R$  are modified *only for the energy equation* by replacing the pressure  $p$  with the total enthalpy per unit mass,  $h_t = E + (p/\rho)$  as :

$$\bar{\alpha}_L = (h_t)_L / (\rho_L c_m), \quad \bar{\alpha}_R = (h_t)_R / (\rho_R c_m).. \quad (35)$$

We observed, in a certain case, better resolution at contact discontinuity using Zha CUSP2 in comparison with the original Zha E-CUSP. However, Eq.(35) violates the above-mentioned consistency of the cell-interface mass flux with the exact Riemann solutions. Hence, we *do not* recommend presently the Zha CUSP2 for general use.

#### 4.4.2 Acoustic flux terms

**(1) Explicit temporal discretization** When the explicit discretization is used, the acoustic flux terms are discretized using the pressure splitting formulations of AUSM+[27] as in the case of the Zha E-CUSP :

$$\mathbf{F}_{1/2}^p = \left( 0, p_{1/2}, (pu)_{1/2} \right)^T, \quad (36)$$

$$p_{1/2} = (\mathcal{P}^+ p)_L + (\mathcal{P}^- p)_R,$$

$$\mathbf{M}_L = u_L / c_{1/2}, \quad \mathbf{M}_R = u_R / c_{1/2},$$

$$c_{1/2} = (1/2)(c_L + c_R),$$

$$(\mathcal{P}^+ p)_L = \begin{cases} p_L \left\{ (1/4)(\mathbf{M}_L + 1)^2 (2 - \mathbf{M}_L) + (3/16) \mathbf{M}_L (\mathbf{M}_L^2 - 1)^2 \right\}, & \text{if } |\mathbf{M}_L| \leq 1; \\ p_L (u_L + |u_L|) / (2 u_L), & \text{otherwise.} \end{cases} \quad (37)$$

$$(\mathcal{P}^- p)_R = \begin{cases} p_R \left\{ (1/4)(\mathbf{M}_R - 1)^2 (2 + \mathbf{M}_R) - (3/16) \mathbf{M}_R (\mathbf{M}_R^2 - 1)^2 \right\}, & \text{if } |\mathbf{M}_R| \leq 1; \\ p_R (u_R - |u_R|) / (2 u_R), & \text{otherwise.} \end{cases} \quad (38)$$

$$(pu)_{1/2} = \begin{cases} p_L u_L, & \text{if } M_L \geq 1; \\ p_R u_R, & \text{if } M_R \leq -1; \\ (1/2)\{p_L(u_L + c_{1/2})\} + (1/2)\{p_R(u_R - c_{1/2})\}, & \text{otherwise.} \end{cases} \quad (39)$$

**(2) Semi-implicit temporal discretization** When the semi-implicit discretization is used, it is only necessary to change the algorithm for the explicit discretization as follows :

(i) Eq.(36) is replaced by the linear interpolation :

$$p_{1/2} = (p_j + p_{j+1})/2, \quad (40)$$

(ii) Eq.(39) is evaluated with

$$p_L = p_R = (p_j + p_{j+1})/2 \quad (41)$$

**4.5 GCUP pressure-correction** At the final stage of the solution procedure, the pressure  $\{p_j\}$  and the cell-averages  $\{\mathbf{Q}_j\}$  are corrected to yield the  $(n+1)$ th time-level solutions,  $\{p_j^{n+1}\}$  and  $\{\mathbf{Q}_j^{n+1}\}$  so as to satisfy the following conditions :

(i) the acoustic part of the flux contributes to  $\{\mathbf{Q}_j^{n+1}\}$  in the following implicit fashion :

$$\mathbf{F}_{1/2}^p = \begin{cases} \left( 0, p_{1/2}^{n+1/2}, (pu)_{1/2}^{n+1/2} \right)^T, & \text{if id\_switch = EX (explicit) ;} \\ \left( 0, p_{1/2}^{n+1}, (pu)_{1/2}^{n+1} \right)^T, & \text{if id\_switch = SI (semi-implicit).} \end{cases} \quad (42)$$

(ii) the  $(n+1)$ th time-level state variables fulfill the given EOS :  $G(p_j^{n+1}, \rho_j^{n+1}, T_j^{n+1}) = 0$ .

The GCUP corrects  $p_j$  and  $\mathbf{Q}_j$  using the following iteration based on the Newton method :

**Initial guess :**

$$p^{(0)} = \begin{cases} p^n, & \text{if id\_switch=EX ;} \\ p^{\text{ad}}, & \text{if id\_switch=SI.} \end{cases}$$

$$\mathbf{Q}^{(0)} = \mathbf{Q}^{n+1*}.$$

**Iterate until finding the limit of recurrence :**

Do  $m = 1, 2, 3, \dots$

- Apply the Newton method to the EOS ( $G(p, \rho, T) = 0$ ) ; solve the following linear system of pressure-correction equations in an elliptic form to obtain  $\{\delta p_j^{(m)}\}$  :

$$\delta G \left( \delta p_{j-1}^{(m)}, \delta p_j^{(m)}, \delta p_{j+1}^{(m)} \right) = - G \left( p_j^{(m-1)}, \rho_j^{(m-1)}, T_j^{(m-1)} \right), \quad j = 1, 2, 3, \dots, N_{\text{cell}}. \quad (43)$$

$\delta G \left( \delta p_{j-1}^{(m)}, \delta p_j^{(m)}, \delta p_{j+1}^{(m)} \right)$  is the variation of  $G$  due to the pressure-correction  $\delta p$ , which is expressed as a linear combination of the pressure-corrections  $\delta p_{j-1}$ ,  $\delta p_j$  and  $\delta p_{j+1}$ . A general and a specific form of  $\delta G$  is derived later in this section. The right-hand side constant is the residual of the EOS with the sign reversed. The linear system of equations Eq.(43) can be solved using the same solver used for Eq.(13).

- Compute  $\delta \mathbf{Q}_j^{(m)} = (\delta \rho_j^{(m)}, \delta \rho u_j^{(m)}, \delta \rho E_j^{(m)})^T$  by substituting the solution of Eq.(43) into the equations representing the relations between  $\delta \mathbf{Q}$  and  $\delta p$  to be derived later. (Eqs.(47), (49) and (51))

- Update  $p$  and  $\mathbf{Q}$  as :

$$p_j^{(m)} = p_j^{(m-1)} + \delta p_j^{(m)} \quad (44)$$

$$\mathbf{Q}_j^{(m)} = \mathbf{Q}_j^{(m-1)} + \delta \mathbf{Q}_j^{(m)}. \quad (45)$$

- Solve the enthalpy relation Eq.(4) with  $\mathbf{Q}_j^{(m)}$  to obtain  $T_j^{(m)}$  :

$$(\rho E)_j^{(m)} - (1/2) \cdot ((\rho u)_j^{(m)})^2 / \rho_j^{(m)} + p_j^{(m)} = \rho_j^{(m)} \cdot h(p_j^{(m)}, \rho_j^{(m)}, T_j^{(m)}). \quad (46)$$

The corrections  $\delta \rho$ ,  $\delta \rho u$  and  $\delta \rho E$  are represented by the pressure-correction as follows :

### (1) momentum-correction

$$\begin{aligned} \delta \rho u_j &= (\delta \rho u_{j-1/2} + \delta \rho u_{j+1/2}) / 2 \approx \left( -\Delta t \cdot \text{grad}(\alpha \cdot \delta p) \Big|_{j-1/2} - \Delta t \cdot \text{grad}(\alpha \cdot \delta p) \Big|_{j+1/2} \right) / 2 \\ &\approx \left\{ -\Delta t \cdot \alpha \cdot (\delta p_j - \delta p_{j-1}) / \Delta x - \Delta t \cdot \alpha \cdot (\delta p_{j+1} - \delta p_j) / \Delta x \right\} / 2, \end{aligned} \quad (47)$$

where  $\alpha = 1/2$  for id\_switch=EX, and  $\alpha = 1$  for id\_switch=SI :  $\alpha = 1/2$  provides the second-order approximation of the pressure corresponding to  $p_{1/2}^{n+1/2}$  in Eq.(42), whereas  $\alpha = 1$  provides the first-order approximation corresponding to  $p_{1/2}^{n+1}$ .

### (2) energy-correction

Several methods to correct the total energy  $\rho E_j$  can be conceived. The simplest one may be expressed as :

$$\delta \rho E_j = -\Delta t \cdot \delta \text{div}(p u) \Big|_j \approx -\Delta t \cdot \delta \text{div}(p \delta u) \Big|_j - \delta \Delta t \cdot \text{div}(u \delta p) \Big|_j. \quad (48)$$

This method straightforward reflects the implicitness on the acoustic part of the flux vector, however, it caused instabilities when applied to low-speed flows. Alternatively, we use the following correction :

$$\begin{aligned} \delta \rho E_j &= -\Delta t \cdot \delta \text{div}(H \rho u) \Big|_j \approx -\Delta t \cdot \text{div}(H \delta \rho u + \rho u \delta H) \Big|_j \\ &\approx -\Delta t \cdot \text{div}(\bar{H} \delta \rho u + \bar{\rho} \bar{u} \delta(\bar{E} + (p/\bar{\rho}))) \Big|_j \\ &\approx -\Delta t \cdot \text{div}(\bar{H} \delta \rho u + \bar{u} \delta p) \Big|_j \\ &\approx -\Delta t \cdot \left\{ \bar{H}_{j+1/2} \delta \rho u_{j+1/2} + \bar{H}_{j-1/2} \delta \rho u_{j-1/2} \right\} / \Delta x - \Delta t \cdot \left\{ \bar{u}_{j+1/2} \delta p_{j+1/2} - \bar{u}_{j-1/2} \delta p_{j-1/2} \right\} / \Delta x \\ &\approx -\Delta t \cdot \left\{ -\bar{H}_{j+1/2} \Delta t \cdot \alpha \cdot (\delta p_{j+1} - \delta p_j) / \Delta x + \bar{H}_{j-1/2} \Delta t \cdot \alpha \cdot (\delta p_j - \delta p_{j-1}) / \Delta x \right\} / \Delta x \\ &\quad - \Delta t \cdot \left\{ \bar{u}_{j+1/2} \alpha \cdot (\delta p_{j+1} + \delta p_j) / 2 - \bar{u}_{j-1/2} \alpha \cdot (\delta p_j + \delta p_{j-1}) / 2 \right\} / \Delta x, \end{aligned} \quad (49)$$

where  $H$  is the total enthalpy per unit mass. In the above equation, the cell-interface total enthalpy,  $\bar{H}_{j+1/2}$ , is assumed to be the weighted-average of  $H_{j+1/2}^n$ ,  $H_{j+1/2}^*$  and  $H_{j+1/2}^{**}$  estimated in each Runge-Kutta stage. In fact, rearranging Eqs.(19a)-(19c), we can obtain the following form of the Runge-Kutta time integration :

$$\mathbf{Q}_j^{n+1*} = \mathbf{Q}_j^n + (1/6)\Delta t \mathcal{L}(\mathbf{Q}^n; j) + (1/6)\Delta t \mathcal{L}(\mathbf{Q}^*; j) + (2/3)\Delta t \mathcal{L}(\mathbf{Q}^{**}; j).$$

Then, roughly evaluating their contribution to the time integration through the energy flux,  $H\rho u$ , we can assume

$$\bar{H}_{j+1/2} = (1/6) \cdot H_{j+1/2}^n + (1/6) \cdot H_{j+1/2}^* + (2/3) \cdot H_{j+1/2}^{**}. \quad (50)$$

Here the cell-interface total enthalpy,  $H_{j+1/2}^n$ ,  $H_{j+1/2}^*$  and  $H_{j+1/2}^{**}$  are approximated in the simple up-wind fashion as :

$$H_{1/2}^\bullet = \begin{cases} E_L^\bullet + p_L^\bullet / \rho_L^\bullet, & \text{if } (\rho u)_{1/2} \geq 0; \\ E_R^\bullet + p_R^\bullet / \rho_R^\bullet, & \text{otherwise.} \end{cases}$$

The velocity at cell-interface  $\bar{u}_{j+1/2}$  is assumed in the similar fashion described above.

### (3) density-correction

The density is corrected in the following fashion taking into account the change of the cell-interface mass flux due to the pressure correction :

$$\begin{aligned} \delta \rho_j &= -\Delta t \cdot \delta \operatorname{div}(\rho u) \Big|_j = -\Delta t \cdot \operatorname{div}(\delta \rho u) \Big|_j \approx -\Delta t \cdot (\delta \rho u_{j+1/2} - \delta \rho u_{j-1/2}) / \Delta x \\ &= -\Delta t \cdot \left\{ -\Delta t \cdot \alpha \cdot (\delta p_{j+1} - \delta p_j) / \Delta x + \Delta t \cdot \alpha \cdot (\delta p_j - \delta p_{j-1}) / \Delta x \right\} / \Delta x. \end{aligned} \quad (51)$$

### Derivation of the general and the specific form of $\delta G$

Here we consider the EOS, and evaluate the variation of the function  $G$  due to the correction  $\delta \mathbf{Q} = (\delta \rho, \delta \rho u, \delta \rho E)^\top$ . At first, consider the differential of Eq.(3) :

$$\delta G_j = \partial_p G \Big|_j \cdot \delta p_j + \partial_\rho G \Big|_j \cdot \delta \rho_j + \partial_T G \Big|_j \cdot \delta T_j. \quad (52)$$

Recall we have assumed that the enthalpy per unit mass,  $h$ , is a known function of  $(p, \rho, T)$ . Taking the differential of Eq.(4), we have

$$\delta \rho E_j - \frac{1}{2} \delta (\rho u^2) \Big|_j + \delta p_j = \partial_p \rho h \Big|_j \cdot \delta p_j + \partial_\rho \rho h \Big|_j \cdot \delta \rho_j + \partial_T \rho h \Big|_j \cdot \delta T_j. \quad (53)$$

Then eliminate  $\delta T$  from Eqs.(52) and (53) to yield

$$\begin{aligned} \delta G_j &= \left[ (\partial_p G) - (\partial_T G) \cdot (\partial_T \rho h)^{-1} \cdot (\partial_p \rho h) + (\partial_T G) \cdot (\partial_T \rho h)^{-1} \right] \Big|_j \cdot \delta p_j \\ &+ \partial_T G \Big|_j \cdot \left( \partial_T \rho h \Big|_j \right)^{-1} \cdot \delta \rho E_j + (\delta \rho - \text{term})_j + (\delta \rho u - \text{term})_j. \end{aligned} \quad (54)$$

In the derivation of Eq.(54), note that  $\delta (\rho u^2)$  can be represented by the correction  $\delta \rho$  and  $\delta \rho u$  as :

$$\delta (\rho u^2) \approx 2u \cdot \delta \rho u - u^2 \delta \rho.$$

Now we have a complete set of corrections for  $\delta \mathbf{Q}_j = (\delta \rho_j, \delta \rho u_j, \delta \rho E_j)^\top$  and  $\delta G_j$  : Eqs.(47), (49), (51) and (54). One may substitute Eqs.(47), (49) and (51) into Eq.(54) to yield the following expression of  $\delta G_j$  as a function of the pressure-correction  $\{\delta p_j\}$  :

$$\begin{aligned}
\delta G_j = & \left[ (\partial_p G) - (\partial_T G) \cdot (\partial_T \rho h)^{-1} \cdot (\partial_p \rho h) + (\partial_T G) \cdot (\partial_T \rho h)^{-1} \right]_j \cdot \delta p_j \\
& + \partial_T G|_j \cdot (\partial_T \rho h|_j)^{-1} \cdot (\Delta t / \Delta x)^2 \cdot \alpha \cdot \left\{ \bar{H}_{j+1/2} \delta p_{j+1} - (\bar{H}_{j+1/2} + \bar{H}_{j-1/2}) \delta p_j + \bar{H}_{j-1/2} \delta p_{j-1} \right\} \\
& - \partial_T G|_j \cdot (\partial_T \rho h|_j)^{-1} \cdot (\Delta t / \Delta x) \cdot \left\{ \bar{u}_{j+1/2} \alpha \cdot (\delta p_{j+1} + \delta p_j) / 2 - \bar{u}_{j-1/2} \alpha \cdot (\delta p_j + \delta p_{j-1}) / 2 \right\} \\
& + (\delta p\text{-terms arising from the } \delta \rho \text{ and the } \delta \rho u\text{-terms of Eq.(54)})_j.
\end{aligned} \tag{55}$$

Then, one might substitute Eq.(55) into Eq.(43), and thereby obtain a pressure-correction equation. However, we recommend to use a simpler expression of  $\delta G_j$  by omitting the third term (arising from the  $\bar{u} \delta p$ -term of Eq.(49)) and the fourth term of the right-hand side of Eq.(55). As the result, we propose the following general form of  $\delta G_j$  :

$$\begin{aligned}
\delta G_j = & \left[ (\partial_p G) - (\partial_T G) \cdot (\partial_T \rho h)^{-1} \cdot (\partial_p \rho h) + (\partial_T G) \cdot (\partial_T \rho h)^{-1} \right]_j \cdot \delta p_j \\
& + \partial_T G|_j \cdot (\partial_T \rho h|_j)^{-1} \cdot (\Delta t / \Delta x)^2 \cdot \alpha \cdot \left\{ \bar{H}_{j+1/2} \delta p_{j+1} - (\bar{H}_{j+1/2} + \bar{H}_{j-1/2}) \delta p_j + \bar{H}_{j-1/2} \delta p_{j-1} \right\},
\end{aligned} \tag{56}$$

which is substituted into the left-hand side of Eq.(43) to yield the pressure-correction equation. The derivatives of  $G$  and  $\rho h$  in the above equation are evaluated by the state variables of  $(m-1)$ th iteration step.

Note that the energy correction itself is computed by Eq.(49) with the  $u \delta p$ -term, though the term is omitted in the pressure-correction equation.

The pressure-correction equation Eq.(43) is reduced for the specific EOS as follows :

#### Pressure-correction equation for the calorically perfect gas EOS

$$\begin{aligned}
& \delta p_j^{(m)} - (\gamma - 1) \cdot (\Delta t / \Delta x)^2 \cdot \alpha \cdot \left\{ \bar{H}_{j+1/2} \delta p_{j+1}^{(m)} - (\bar{H}_{j+1/2} + \bar{H}_{j-1/2}) \delta p_j^{(m)} + \bar{H}_{j-1/2} \delta p_{j-1}^{(m)} \right\} \\
& = -p_j^{(m-1)} + (\gamma - 1) \left( \rho_j^{(m-1)} E_j^{(m-1)} - (1/2) (\rho_j^{(m-1)} u_j^{(m-1)})^2 / \rho_j^{(m-1)} \right).
\end{aligned} \tag{57}$$

#### Pressure-correction equation for the Tammann EOS

$$\begin{aligned}
& \delta p_j^{(m)} - (\gamma_c - 1) \cdot (\Delta t / \Delta x)^2 \cdot \alpha \cdot \left\{ \bar{H}_{j+1/2} \delta p_{j+1}^{(m)} - (\bar{H}_{j+1/2} + \bar{H}_{j-1/2}) \delta p_j^{(m)} + \bar{H}_{j-1/2} \delta p_{j-1}^{(m)} \right\} \\
& = -p_j^{(m-1)} - \gamma_c p_0 + (\gamma_c - 1) \left( \rho_j^{(m-1)} E_j^{(m-1)} - (1/2) (\rho_j^{(m-1)} u_j^{(m-1)})^2 / \rho_j^{(m-1)} \right).
\end{aligned} \tag{58}$$

**5. Numerical experiments** In this section, we evaluate the accuracy, efficiency and robustness of the MUSE/E-CUSP\_GCUP method derived above. A series of one-dimensional Riemann (or shock-tube) problem is computed. In addition, the switching between the semi-implicit and explicit discretizations is demonstrated with solving a subsonic-to-supersonic flow transient problem.

For the Riemann problems, the initial data is composed of two uniform states separated by a discontinuity at the origin :

$$\mathbf{Q}(x, t) = (\rho, (\rho u), (\rho E))^T = \begin{cases} \mathbf{Q}_L, & \text{if } x < 0 ; \\ \mathbf{Q}_R, & \text{if } x > 0. \end{cases}$$

**5.1 Riemann problems** A series of one-dimensional Riemann problems is solved. The followings are given as common input setup in this paper :

maximum allowable  $CFL_{\text{acos}}$  for the explicit discretization :

$$\sigma_{\text{max}} = \begin{cases} 0.4 & \text{for perfect gas EOS ;} \\ 0.4 & \text{for liquid (Tammann) EOS, supersonic flows ;} \\ 0.1 & \text{for liquid (Tammann) EOS, subsonic flow .} \end{cases}$$

maximum allowable  $CFL_{\text{conv}}$  for the semi-implicit discretization :  $\tau_{\text{max}} = 0.2$ .

The convergence criteria for the GCUP iteration in the present computations are given as follows :

$$\begin{aligned} \max_j |\delta p_j^{(m)} / p_j^{(m)}| &< 10^{-5}, & \max_j |\delta \rho_j^{(m)} / \rho_j^{(m)}| &< 10^{-5}, \\ \max_j |\delta \rho u_j^{(m)} / (\rho u_j^{(m)} + 1)| &< 10^{-5}, & \max_j |\delta \rho E_j^{(m)} / \rho E_j^{(m)}| &< 10^{-5}, \\ \max_j |G(p_j^{(m)}, \rho_j^{(m)}, T_j^{(m)}) / p_j^{(m)}| &< 10^{-5}. \end{aligned}$$

The compression parameter  $\beta$  of the slope limiter in Eq.(24) is assumed to be 4.

Representative test cases are summarized in Table 5.1.1. This table shows EOS (equation of state) used, initial left and right state, grid spacing  $\Delta x$ , the termination time  $t_{\text{end}}$ , the temporal discretization denoted by ‘EX’ and ‘SI’ (indicating explicit and semi-implicit, respectively), the maximum local Mach number over the computational domain, the maximum acoustic CFL number  $\max CFL_{\text{acos}j}$ , and the maximum convective CFL number  $\max CFL_{\text{conv}j}$ . Results for ‘EX’ case are obtained with input  $M_{\text{sw}} = 0$  ; ‘SI’ case with  $M_{\text{sw}} = 10^{20}$ . All cases listed in Table 5.1.1 are solved using the GCUP.

**5.1.1 Accuracy and stability** From case1 to case9 we tested on the calorically perfect gas EOS with  $\gamma = 1.4$ . Case1 and case2 are the standard benchmark problem by Sod[28]. The maximum Mach number is 0.93, and  $\max CFL_{\text{acos}j}$  of case1 (‘EX’) and case2 (‘SI’) becomes the same order of magnitude under the given restriction on  $\sigma_{\text{max}}$  and  $\tau_{\text{max}}$ . The solutions for these cases are depicted in Fig 5.1.1 and Fig.5.1.2 in comparison with theoretical solutions. Case1 shows the desired solution as long as one can hope to the third-order finite-volume method. Case2 shows high resolution for the shock and contact discontinuity, however an oscillation takes place at the tail of the rarefaction wave. To examine accuracy of the third-order reconstruction, see Fig.5.1.3 where the results of the first-order reconstruction with the explicit discretization are illustrated for the sake of comparison.

Case3 and case4 are the standard benchmark by Lax[29]. The best of the class accurate solutions are obtained by both the explicit and semi-implicit discretizations as shown in Fig.5.1.4 and Fig.5.1.5. The solutions using the semi-implicit discretization shown in Fig.5.1.5 are even more favorable. A comparison with the AUSM+ has been performed under the same condition as case3. Figure 5.1.6 shows results obtained using the AUSM+ illustrating virtually the same solution as the present method.

Case5 and case6 are involved with a Riemann problem cited from [1], in which the solution contains two shock waves. Fig.5.1.8 is the solution for case6, which shows the semi-implicit discretization produces a result comparable to the explicit. Evaluation for these cases are similar to that for case3 and

case4.

Case7 and case8 are intended for a low-speed flow, and the solutions are shown in Fig.5.1.9 and Fig.5.1.10. The maximum local Mach number is small, see Table 5.1.1, thus in case8, the maximum acoustic CFL number becomes much larger than 1. Despite such a large departure from the CFL condition, the semi-implicit discretization is quite stable. The contact discontinuity is well captured with high-resolution. This implies that high accuracy for the convective transport is still preserved using the semi-implicit discretization. Significant dissipation on the shock and the rarefaction wave is the price to pay for the advantage to taking a large time step that breaks the CFL condition. The shock and the rarefaction in Fig.5.1.10 are much less smeared than in Fig.5.1.9. However, due to the CFL condition, the explicit discretization needs a large number of time steps (5942), thus the inevitable accumulation of the numerical dissipation in each time step contaminates the solution.

Case9 is another example of low-speed flow. In this case, the maximum local Mach number is in the order of  $10^{-4}$ , which corresponds, for instance, to natural convection flows. The solutions are shown in Fig.5.1.11.

From case10 to case15, we tested on the Tammann EOS simulating the characteristics of the liquid water. The data for the densities, pressures and velocities are determined using SI units, e.g. the initial left state of case10 is  $(p_L, \rho_L, u_L) = (10^9 \text{ Pa}, 1436 \text{ kg/m}^3, 0 \text{ m/s})$ . Sound speeds in liquids are generally so high that, for instance in case9 and case10, the velocity reaches 200m/s, which is very high speed for liquids in the usual sense, but the maximum local Mach number is only 0.1. The solutions are shown in Figs.5.1.12-13 and Figs.5.1.15-18. Outline of our observation on the solutions of these cases including a supersonic flow (case15) is similar to that for the perfect gas EOS, and thus is not recalled herein. To examine the accuracy of the third-order reconstruction in computing the convective flux terms, see the results of the first-order reconstruction shown in Fig.5.1.14 for comparison with case10.

All the solutions introduced above are obtained using the GCUP. We have confirmed that the solutions with and without using the GCUP are virtually identical when we use the explicit temporal discretization. However, as for the semi-implicit discretization, when we don't use the GCUP, we failed to obtain solutions in the cases listed in Table 5.1.2. The spurious oscillation occurred in case9a is depicted in Fig.5.1.19.

**5.1.2 Efficiency** The computation time for each case is summarized in Table 5.1.3. In this table, 'GCUP iter.' is the number of iteration performed in the GCUP, and 'Ratio EX/SI' is the ratio of the computation time of the explicit case to that of the corresponding semi-implicit case. For high-speed regime where  $\max M_j$  is larger than around 1, the computation times of explicit cases are comparable to or less than those of the semi-implicit cases. In low-speed regime, the semi-implicit discretization dominates with decreasing the Mach number. The semi-implicit case for  $\max M_j = O(10^{-3})$  is more than 100 times faster than the explicit case.

**5.2 Flow transient due to a local heat generation** The initial data are taken as :

$$\left( p_L, \rho_L, u_L \right) = \left( 0.1001, 0.01, 0.1 \right) \quad ; \quad \left( p_R, \rho_R, u_R \right) = \left( 0.1, 0.01, 0.1 \right).$$

A time-dependent local heat generation rate is given as :

$$S(t, x) = \begin{cases} \exp(5 \cdot t^2) - 1 & \text{if } (t, x) \in [0.1, \infty] \times [-1, 1]; \\ 0 & \text{otherwise.} \end{cases}$$

As for the Mach number to switch semi-implicit/explicit discretization,  $M_{sw} = 0.8$  is given. The calorically perfect gas EOS with  $\gamma = 1.4$  is used. The grid spacing is  $\Delta x = 0.005$ .

At the initial stage, the maximum local Mach number ( $\max M_j$ ) is 0.027, thus the semi-implicit discretization is activated. The expansion of the gas due to the heat generation results in rapid increase in the gas velocity, and  $\max M_j$  exceeds  $M_{sw}$  at  $t = 0.734$ . At this time, the explicit discretization is activated, and the time step changes from  $\Delta t = 1.771 \times 10^{-4}$  to  $\Delta t = 1.112 \times 10^{-4}$ . The density, the pressure, the velocity and the Mach number at  $t = 0.734$  and  $t = 1$  are shown in Fig.5.2.1. The maximum local Mach number reaches 1.64 at  $t = 1$ , and shock fronts have been formed. The histories of the maximum CFL numbers and  $\max M_j$  are illustrated in Fig.5.2.2. The switching from the semi-implicit discretization to the explicit is smooth, and does not have any adverse effect on the computation.

## 6. Summary and discussion

We have constructed the hybrid semi-implicit/explicit numerical framework MUSE, into which we have incorporated the Zha E-CUSP with the third-order MUSCL reconstruction and the third-order TVD Runge-Kutta time integration. The GCUP is applied in order to deal with flows governed by arbitrary equations of state. The MUSE/E-CUSP\_GCUP method has been confirmed to be accurate and efficient over the wide Mach number range : from  $M=O(10^{-4})$  to supersonic for both gas and liquid flows. The method is strictly conservative, since it is based on the finite-volume approach, so that correct propagations of shock, rarefaction wave and contact discontinuity are guaranteed. We developed the pressure prediction method with incorporating the non-oscillatory second-order projection algorithm by Nessyahu and Tadmor to enforce the pressure-velocity coupling. Despite using non-staggered grids, the present method does not suffer from the well-known oscillation issue in incompressible regime due to the odd-even decoupling in the pressure. Hence, the MUSE/E-CUSP\_GCUP is reliable for both the highly compressible and incompressible flow regimes. The Zha E-CUSP is simple, accurate and robust, so that we can recommend it. Other schemes of the CUSP-family such as AUSM+ may also be available as alternatives to the E-CUSP.

We elaborated the semi-implicit discretization to preserve non-oscillatory solutions in low-speed flows without being constrained by the CFL condition. For the semi-implicit discretization, the implicit formulation for the acoustic flux vector,  $\mathbf{F}_{1/2}^p = (0, p_{1/2}^{n+1}, (pu)_{1/2}^{n+1})^T$  in Eq.(42), is employed. This choice results in a strong suppression on the possible oscillation around the shocks and rarefaction waves, however these waves are significantly smeared out as shown in the numerical experiments on the Riemann problems. One might consider that using higher order implicit discretizations on the acoustic flux vector would improve the resolution for shocks and rarefactions. In fact, second-order implicit discretizations may improve accuracy without occurrence of spurious oscillation when  $CFL_{acos}$  is relatively small. However, we have a pessimistic view that they incur serious oscillations with increasing  $CFL_{acos}$  irrespective of  $CFL_{conv}$ . When the explicit discretization is used with the

GCUP, the acoustic flux vector becomes  $\mathbf{F}_{1/2}^p = (0, p_{1/2}^{n+1/2}, (pu)_{1/2}^{n+1/2})^T$  as in Eq.(42), therefore a second-order implicit discretization takes place. This case also suffers from oscillations if we violate the acoustic CFL condition even if the convective CFL number is much smaller than one.

We have proposed the GCUP formulation in a general form. According to our numerical experiments, we have confirmed that the GCUP has crucial effect on stabilizing the solution when the semi-implicit discretization is used, particularly for low-speed liquid flows. In contrast, when the explicit discretization is used, we could recommend to skip the GCUP so far as the present numerical experiments are concerned. The GCUP part required 30% to 50% of the total computation time for the explicit cases, therefore if we could skip the GCUP, the efficiency goes up considerably. The perfect gas and Tammann EOS employed in this paper consists of the smooth functions. Hence, if the time step is small enough to satisfy the acoustic CFL condition, the magnitude of the pressure-correction,  $\delta p$ , may be negligibly small, and the GCUP may not be required. However, when we are involved with more complex or non-smooth EOS, we may need the GCUP even for the explicit discretization.

The extension to multi-dimensions and the implementation of diffusion terms in the MUSE framework are now under study. Application and validation of the proposed formula of the GCUP upon real-world fluids should be addressed for future work.

## References

- [ 1 ] LeVeque, R. J., "Finite Volume Methods for Hyperbolic Problems," Cambridge University Press, 2002.
- [ 2 ] Turkel, E., "Preconditioned methods for solving incompressible and low speed compressible equations," J. Comput. Phys. **72** (1987) pp. 277-298.
- [ 3 ] Choi, Y.-H., Merkle, C. L., "The application of preconditioning in viscous flows," J. Comput. Phys. **105** (1993) pp. 207-223.
- [ 4 ] Weiss, J. M., Smith, W. A. "Preconditioning applied to variable and constant density time-accurate flows on unstructured meshes," AIAA Paper 94-2209, 1994.
- [ 5 ] Keshtiban, I. J., Belblidia, F. and Webster, M. F., "Compressible flow solvers for low Mach number flows - a review," <http://www.cs.swan.ac.uk/reports/yr2004/CSR2-2004.pdf>, 2004.
- [ 6 ] Harlow, F. H. and Amsden, A., "A numerical fluid dynamics calculation method for all flow speeds," J. Comput. Phys. **8** (1971) pp. 197-213.
- [ 7 ] Patankar, S. V., "Numerical heat transfer and fluid flow," Hemisphere Publishing, 1980.
- [ 8 ] Yabe, T., Xiao, F., Utsumi, T., "The constrained interpolation profile method for multiphase analysis," J. Comput. Phys. **169** (2001) pp. 556-593.
- [ 9 ] Evje, S. and Flatten, T., "Weakly implicit numerical schemes for a two-fluid model," SIAM J. Sci. Comput. **26** (2005) pp. 1449-1484.
- [10] van der Heul, D. R., Vuik, C. and Wesseling, P., "A conservative pressure-correction method for flow at all speeds," Computers & Fluids **32** (2003) pp. 1113-1132.
- [11] Roe, P., "Approximate Riemann solvers, parameter vectors, and difference schemes," J. Comput. Phys., **43**, (1981) pp. 357-372.
- [12] Jameson, A., "Analysis and design of numerical schemes for gas dynamics II: Artificial diffu-

- sion and discrete shock structure,” *Journal of Computational Fluid Dynamics*, **5** (1995) pp. 1-38.
- [13] Liou, M.-S., “Ten years in the making – AUSM-family,” AIAA-2001-2521, 2001.
- [14] Zha, G.-C. and Hu, Z., “Calculation of transonic internal flows using an efficient high resolution upwind scheme,” AIAA Paper 2004-1097, 2004.
- [15] Zha, G.-C., “A low diffusion E-CUSP upwind scheme for transonic flows,” AIAA Paper 2004-2707, 2004.
- [16] Hu, Z. and Zha, G.-C., “Simulation of 3D flows of propulsion systems using an efficient low diffusion E-CUSP upwind scheme,” AIAA Paper 2004-4082 (2004).
- [17] Toda, S., Watanabe, K., Utsumi, T., Akamatsu, M. and Fujii, S., “Two-phase flow computations using GCUP and level-set method,” (in Japanese) Proc. of the 2000 annual conference of Japan SIAM, lecture No.OS 1-3 (2000).
- [18] Gallouët, T., Hérard, J.-M., Seguin, N., “Some recent finite volume schemes to compute Euler equations using real gas EOS,” *Int. J. Numer. Meth. Fluids*, **39** (2002), pp. 1073-1138.
- [19] van der Vorst, H. A., “Iterative Krylov methods for large linear systems,” Cambridge Univ. press (2003).
- [20] Nessyahu, H. and Tadmor, E., “Non-oscillatory central differencing for hyperbolic conservation laws,” *J. Comput. Phys.*, **87** (1990), pp.408-463.
- [21] Jiang, G.-S., Levy D., Lin C.-T., Osher, S. and Tadmor, E., “High-resolution nonoscillatory central schemes with nonstaggered grids for hyperbolic conservation laws,” *SIAM J. Numer. Anal.*, **35** (1998), pp. 2147-2168.
- [22] Shu C.-W. and Osher, S., “Efficient implementation of essentially non-oscillatory shock capturing schemes,” *J. Comput. Phys.* **77** (1988) pp. 439-471.
- [23] van Leer, B., “Towards the ultimate conservative difference scheme, V. A second order sequel to Godunov’s method,” *J. Comput. Phys.*, **32** (1979) pp.101-136.
- [24] Chakravarthy, S. R. and Osher, S., “Computing with high-resolution upwind schemes for hyperbolic equations,” *Lectures in Applied Mathematics* 22 (1985) p. 57-86.
- [25] Hirsch, C., “Numerical computation of internal and external flows, volume 2, Computational methods for inviscid and viscous flows,” Wiley (1990).
- [26] Wada, Y. and Liou, M.-S., “A flux splitting scheme with high-resolution and robustness for discontinuities,” AIAA-94-0083, 1994.
- [27] Liou, M.-S., “Progress towards an improved CFD methods : AUSM+,” AIAA-95-1701-CP, 1995.
- [28] Sod, G. A., “A survey of several finite difference methods for systems of nonlinear conservation laws,” *J. Comput. Phys.*, **27** (1978) pp. 1-31.
- [29] Lax, P. D., “Weak solutions of nonlinear hyperbolic equations and their numerical approximations,” *Comm. Pure Appl. Math.*, **7** (1954) pp. 159-193.

Table 5.1.1 Numerical experiments on Riemann problems.

Case	EOS	$(p_L, \rho_L, u_L)$	$(p_R, \rho_R, u_R)$	$\Delta x$	$t_{\text{end}}$	SI/EX	Mach#	$\max \text{CFL}_{\text{acos } j}$	$\max \text{CFL}_{\text{conv } j}$
1	perfect gas	(1, 1, 0)	(0.1, 0.125, 0)	0.01	0.4	EX	0.93	$\sigma_{\text{max}}(0.4)$	0.169
2	perfect gas	(1, 1, 0)	(0.1, 0.125, 0)	0.01	0.4	SI	0.93	0.447	$\tau_{\text{max}}(0.2)$
3	perfect gas	(3.528, 0.445, 0.698)	(0.571, 0.5, 0)	0.0025	0.12	EX	0.94	$\sigma_{\text{max}}(0.4)$	0.132
4	perfect gas	(3.528, 0.445, 0.698)	(0.571, 0.5, 0)	0.0025	0.12	SI	0.94	0.607	$\tau_{\text{max}}(0.2)$
5	perfect gas	(1, 1, 3)	(1, 2, 1)	0.01	0.5	EX	2.54	$\sigma_{\text{max}}(0.4)$	0.288
6	perfect gas	(1, 1, 3)	(1, 2, 1)	0.01	0.5	SI	2.54	0.279	$\tau_{\text{max}}(0.2)$
7	perfect gas	(1, 1, 0)	(0.99, 0.99, 0)	0.005	10	EX	$3.59 \times 10^{-3}$	$\sigma_{\text{max}}(0.4)$	$1.43 \times 10^{-3}$
8	perfect gas	(1, 1, 0)	(0.99, 0.99, 0)	0.005	10	SI	$3.59 \times 10^{-3}$	55.9	$\tau_{\text{max}}(0.2)$
9	perfect gas	(1, 1, 0)	(0.999, 0.999, 0)	0.005	10	SI	$3.57 \times 10^{-4}$	535	$\tau_{\text{max}}(0.2)$
10	Tammann	$(10^9, 1436, 0)$	$(10^5, 979.5, 0)$	10	1	EX	0.104	$\sigma_{\text{max}}(0.1)$	$7.88 \times 10^{-3}$
11	Tammann	$(10^9, 1436, 0)$	$(10^5, 979.5, 0)$	10	1	SI	0.104	2.51	$\tau_{\text{max}}(0.2)$
12	Tammann	$(10^7, 1000, 0)$	$(10^5, 1000, 0)$	1	1	EX	$2.27 \times 10^{-3}$	$\sigma_{\text{max}}(0.1)$	$2.26 \times 10^{-4}$
13	Tammann	$(10^7, 1000, 0)$	$(10^5, 1000, 0)$	1	1	SI	$2.27 \times 10^{-3}$	88.6	$\tau_{\text{max}}(0.2)$
14	Tammann	$(10^6, 1000, 0)$	$(10^5, 1000, 0)$	1	1.14	SI	$2.09 \times 10^{-4}$	854	$\tau_{\text{max}}(0.2)$
15	Tammann	$(5 \times 10^8, 10^3, 2000)$	$(10^6, 10^3, 2000)$	0.01	$10^{-4}$	EX	1.36	$\sigma_{\text{max}}(0.4)$	0.194

Table 5.1.2 Cases resulted in failure or suffered from serious numerical oscillations.

Case	EOS	$(p_L, \rho_L, u_L)$	$(p_R, \rho_R, u_R)$	$\Delta x$	$t_{\text{end}}$	SI/EX	GCUP	Result
9a	perfect gas	(1, 1, 0)	(0.999, 0.999, 0)	0.005	1	SI	<b>not used</b>	oscillation near contact
11a	Tammann	$(10^9, 1436, 0)$	$(10^5, 979.5, 0)$	10	---	SI	<b>not used</b>	negative pressure
13a	Tammann	$(10^7, 1000, 0)$	$(10^5, 1000, 0)$	1	---	SI	<b>not used</b>	negative pressure
14a	Tammann	$(10^6, 1000, 0)$	$(10^5, 1000, 0)$	1	---	SI	<b>not used</b>	negative pressure

Table 5.1.3 Summary of computation time.

Case	EOS	$(p_L, \rho_L, u_L)$	$(p_R, \rho_R, u_R)$	SI/EX	Mach#	GCUPiter.	Comput.time	RatioEX/SI
1	perfect gas	(1, 1, 0)	(0.1, 0.125, 0)	EX	0.93	4	6	~ 1
2	perfect gas	(1, 1, 0)	(0.1, 0.125, 0)	SI	0.93	3	6	
3	perfect gas	(3.528, 0.445, 0.698)	(0.571, 0.5, 0)	EX	0.94	4	6	~ 1
4	perfect gas	(3.528, 0.445, 0.698)	(0.571, 0.5, 0)	SI	0.94	4	6	
5	perfect gas	(1, 1, 3)	(1, 2, 1)	EX	2.54	3-4	13	0.59
6	perfect gas	(1, 1, 3)	(1, 2, 1)	SI	2.54	3	22	
7	perfect gas	(1, 1, 0)	(0.99, 0.99, 0)	EX	$3.59 \times 10^{-3}$	2	1227	102
8	perfect gas	(1, 1, 0)	(0.99, 0.99, 0)	SI	$3.59 \times 10^{-3}$	2	12	
9	perfect gas	(1, 1, 0)	(0.999, 0.999, 0)	SI	$3.57 \times 10^{-4}$	2	---	
10	Tammann	$(10^9, 1436, 0)$	$(10^5, 979.5, 0)$	EX	0.104	3	615	13.7
11	Tammann	$(10^9, 1436, 0)$	$(10^5, 979.5, 0)$	SI	0.104	5	45	
12	Tammann	$(10^7, 1000, 0)$	$(10^5, 1000, 0)$	EX	$2.27 \times 10^{-3}$	2	3123	521
13	Tammann	$(10^7, 1000, 0)$	$(10^5, 1000, 0)$	SI	$2.27 \times 10^{-3}$	3	6	
14	Tammann	$(10^6, 1000, 0)$	$(10^5, 1000, 0)$	SI	$2.09 \times 10^{-4}$	3	---	
15	Tammann	$(5 \times 10^8, 10^3, 2000)$	$(10^6, 10^3, 2000)$	EX	1.36	4	---	

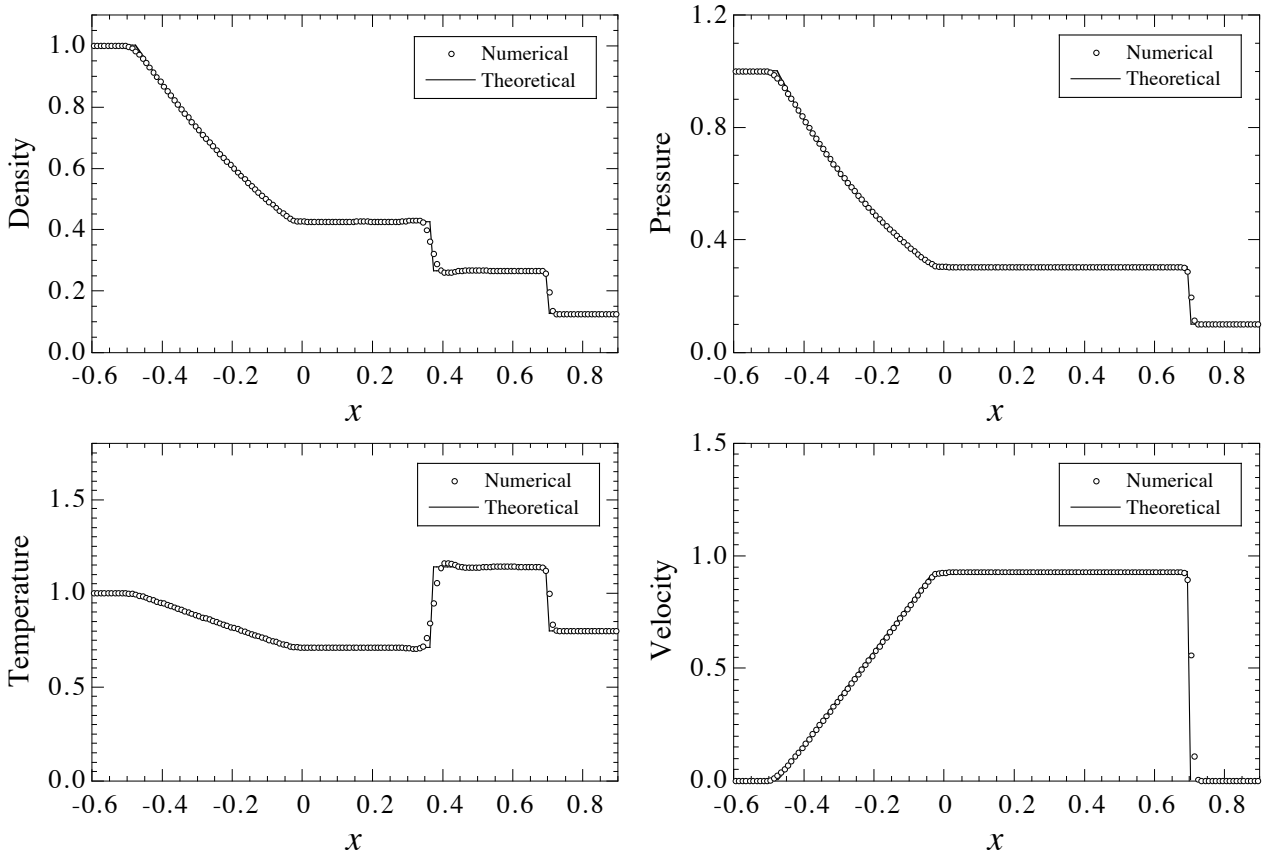


Fig. 5.1.1 Results of case1 (the Sod's problem, EX, perfect gas)

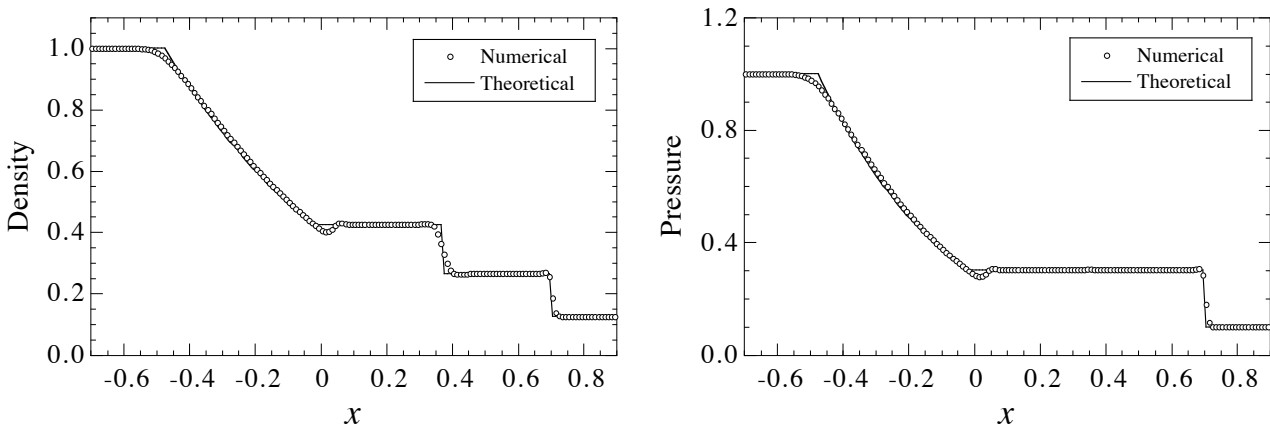


Fig. 5.1.2 Results of case2 (the Sod's problem, SI, perfect gas)

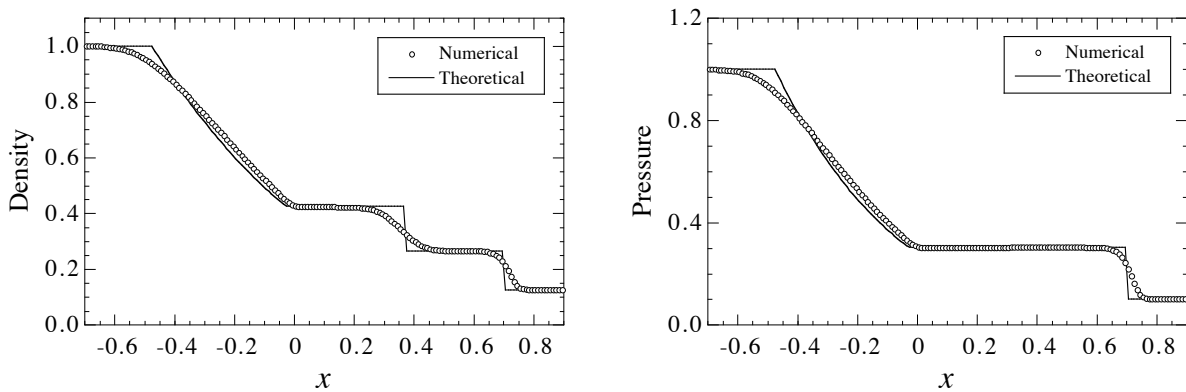


Fig. 5.1.3 Results of the *first-order reconstruction* (the Sod's problem, EX, perfect gas)

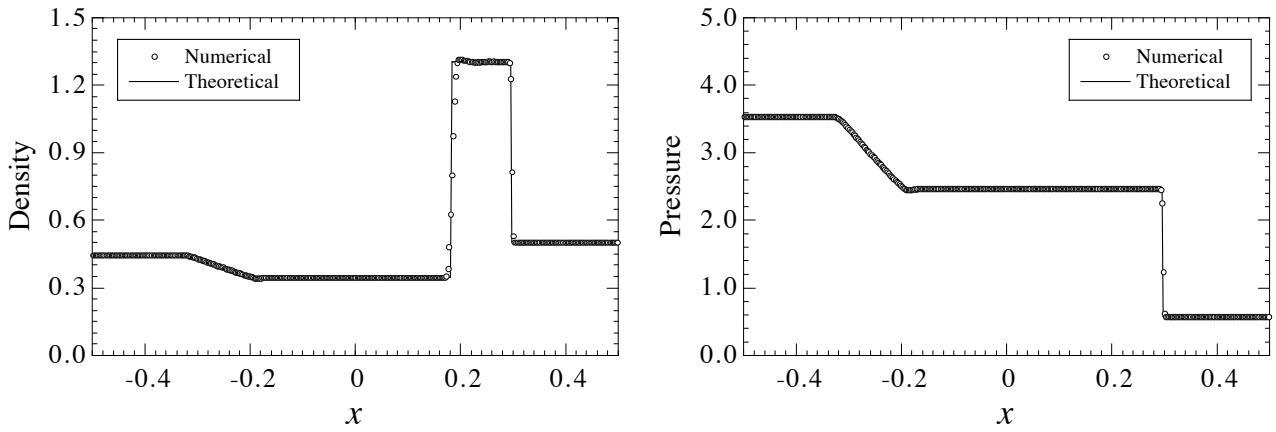


Fig.5.1.4 Results of case3 (the Lax's problem, EX, perfect gas)

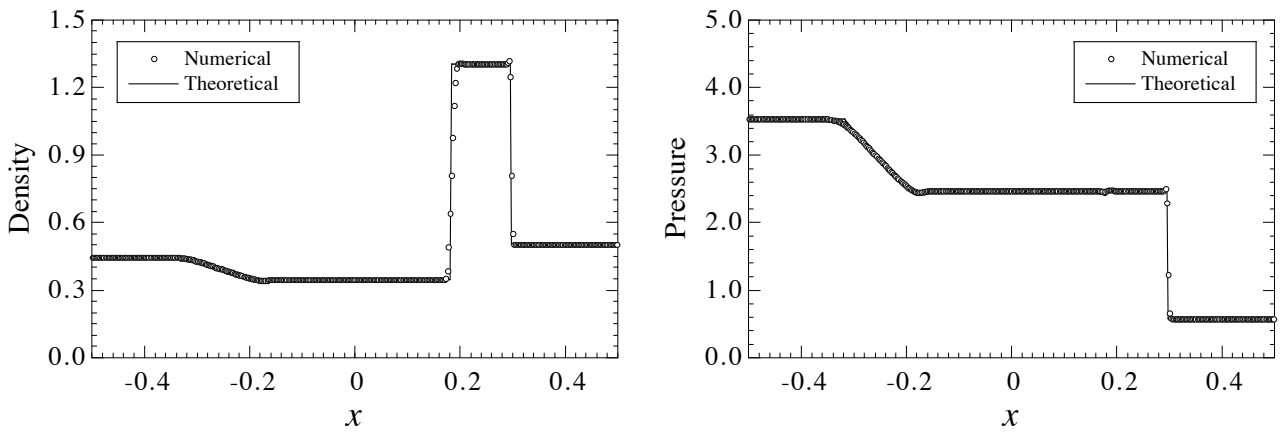


Fig.5.1.5 Results of case4 (the Lax's problem, SI, perfect gas)

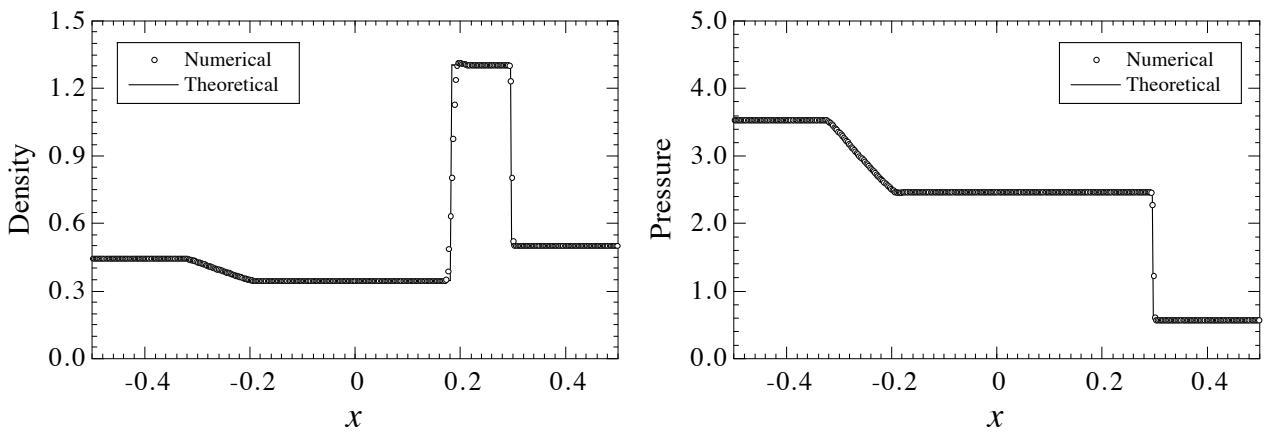


Fig.5.1.6 Results for the Lax's problem using AUSM+ (EX, perfect gas)

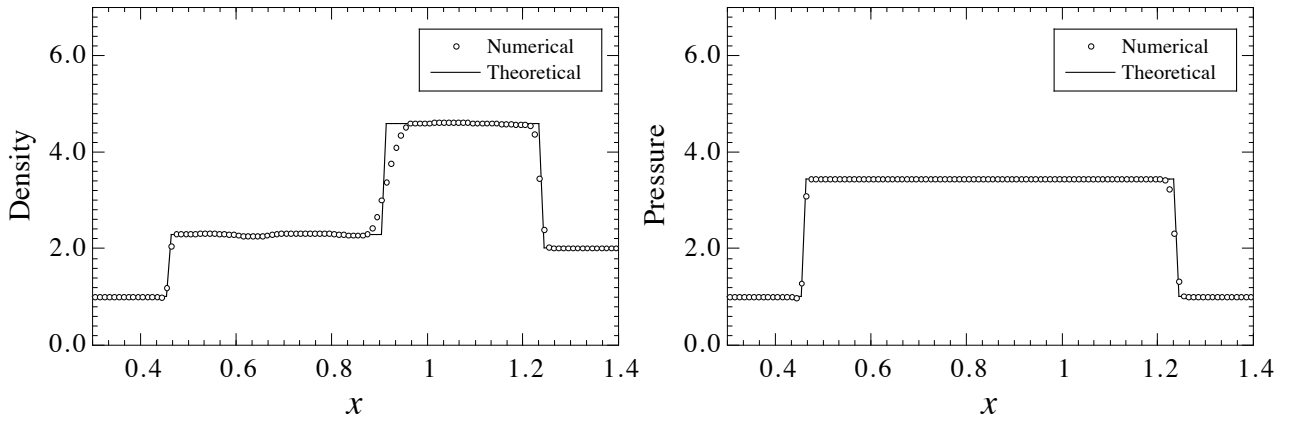


Fig.5.1.7 Results of case5 (double shock, EX, perfect gas)

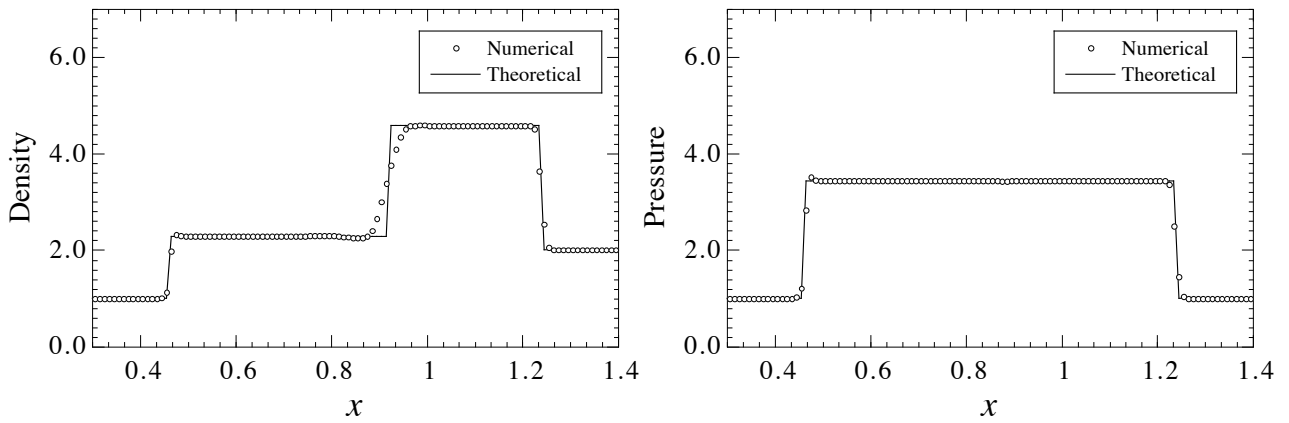


Fig.5.1.8 Results of case6 (double shock, SI, perfect gas)

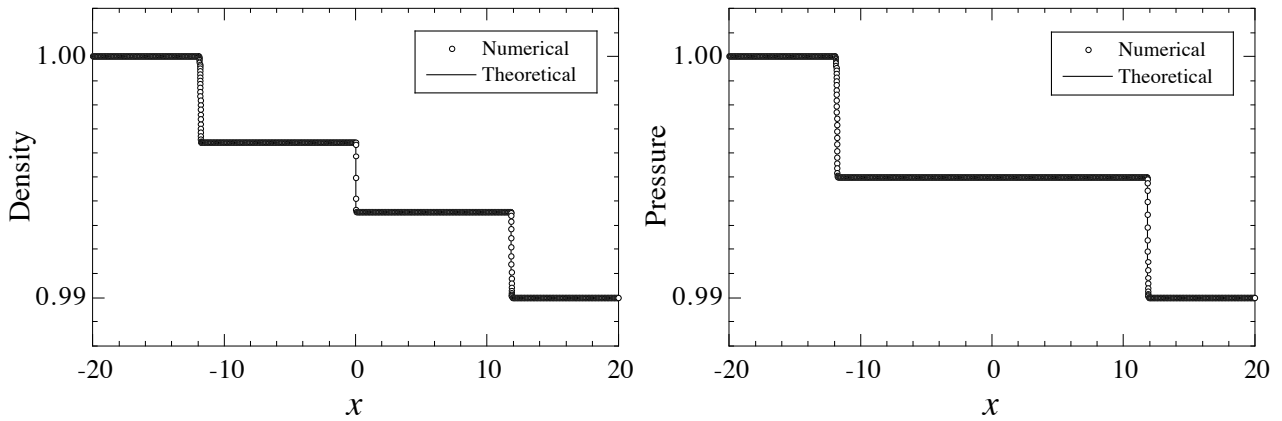


Fig.5.1.9 Results of case7 ( $p_R/p_L = 0.99$ , EX, perfect gas)

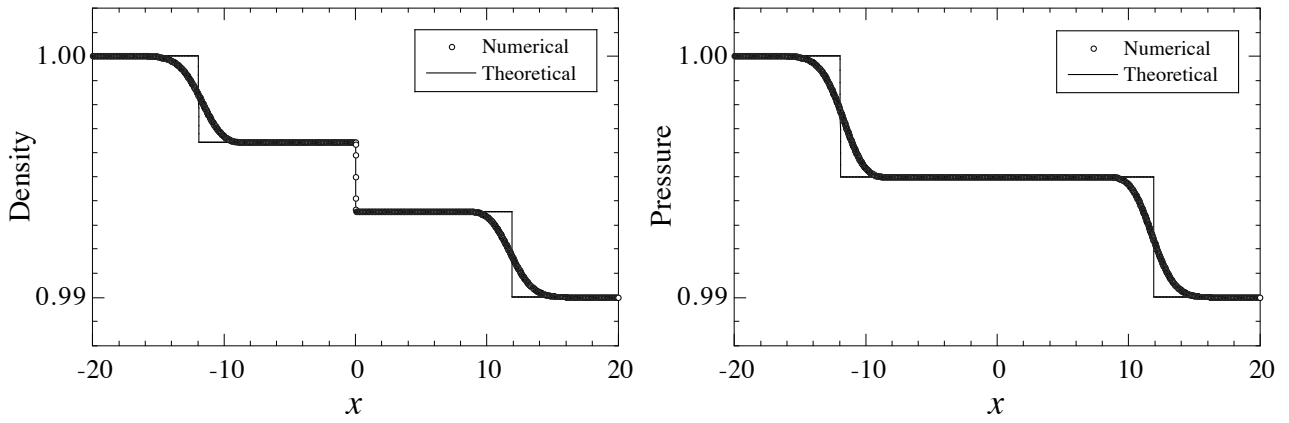


Fig.5.1.10 Results of case8 ( $p_R/p_L = 0.99$ , SI, perfect gas)

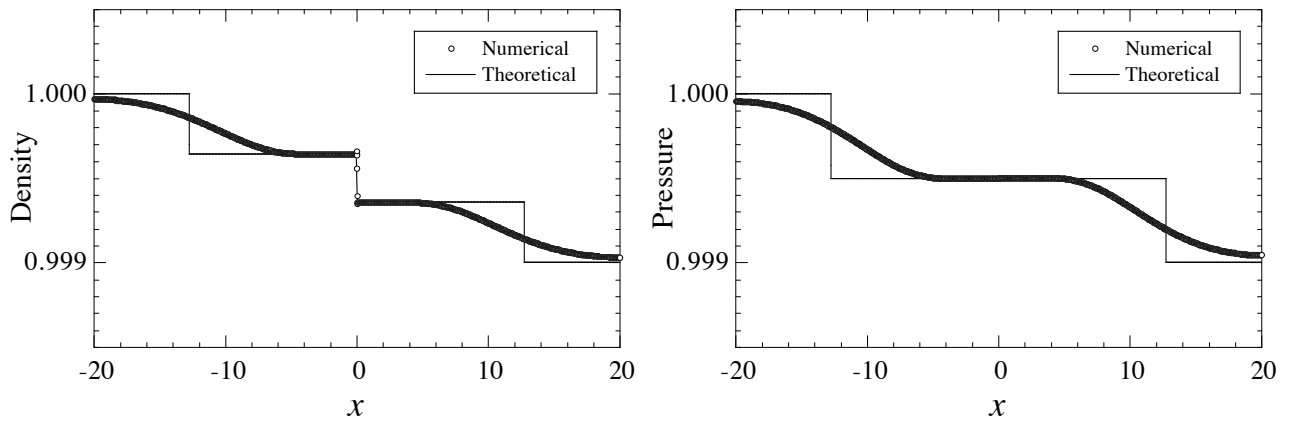


Fig.5.1.11 Results of case9 ( $p_R/p_L = 0.999$ , SI, perfect gas)

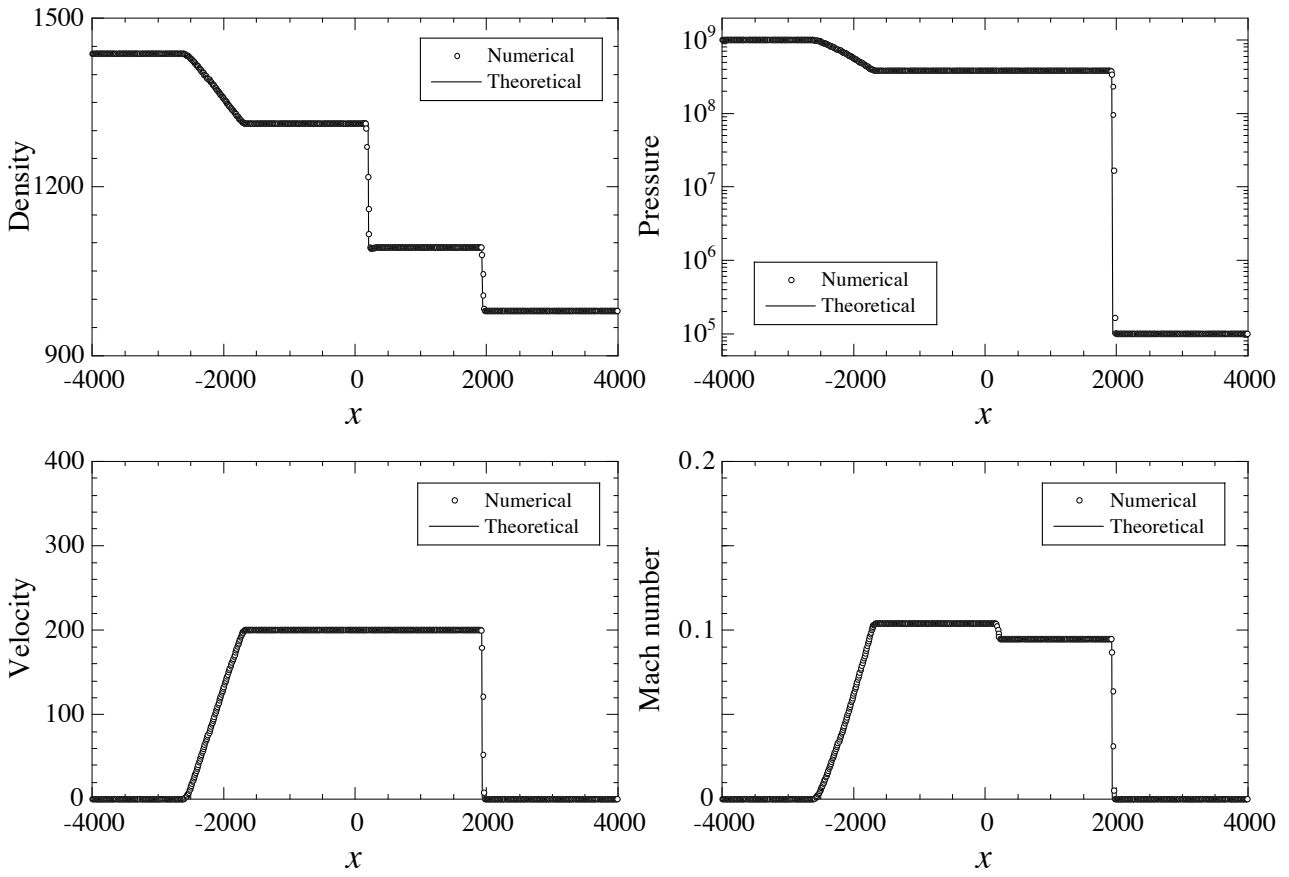


Fig.5.1.12 Results of case10 ( $p_R/p_L = 10^{-4}$ , EX, Tammann EOS)

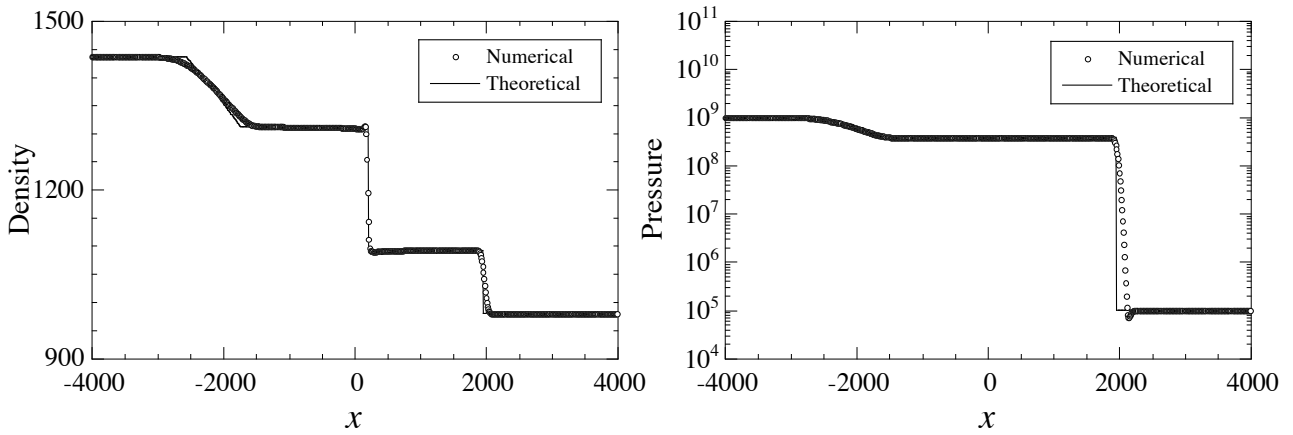


Fig.5.1.13 Results of case11 ( $p_R/p_L = 10^{-4}$ , SI, Tammann EOS)

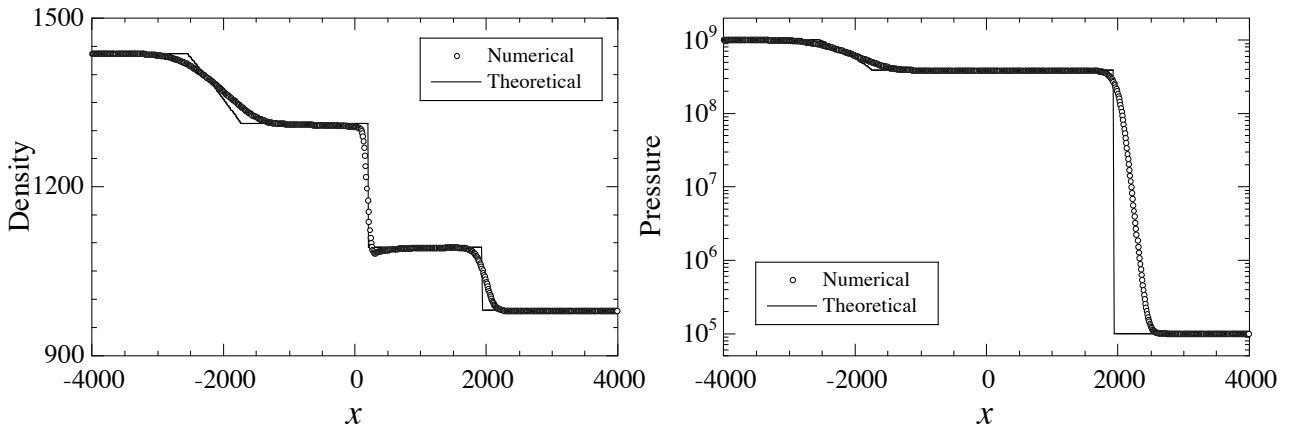


Fig.5.1.14 Results of the *first-order reconstruction* ( $p_R/p_L = 10^{-4}$ , EX, Tammann EOS)

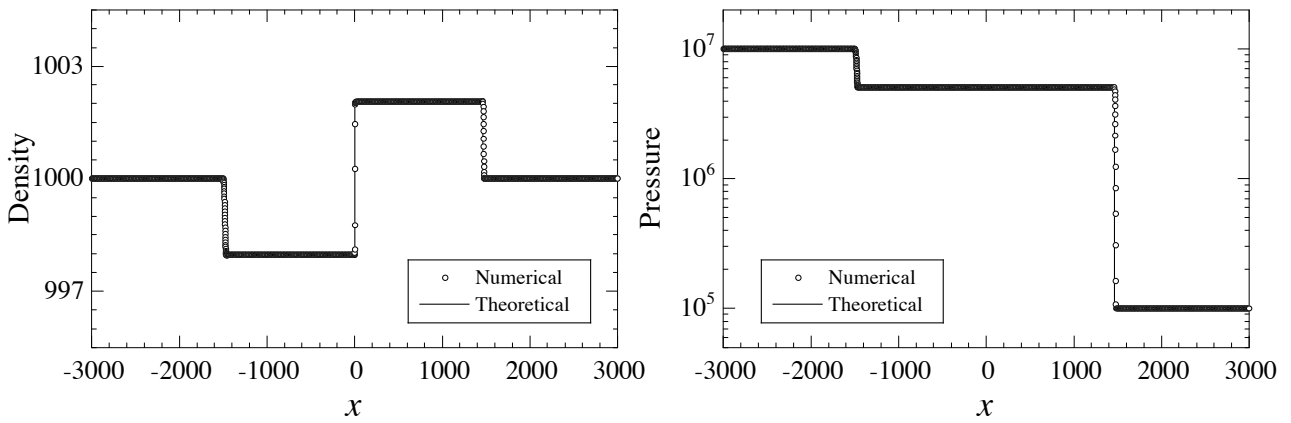


Fig.5.1.15 Results of case12 ( $p_R/p_L = 10^{-2}$ , EX, Tammann EOS)

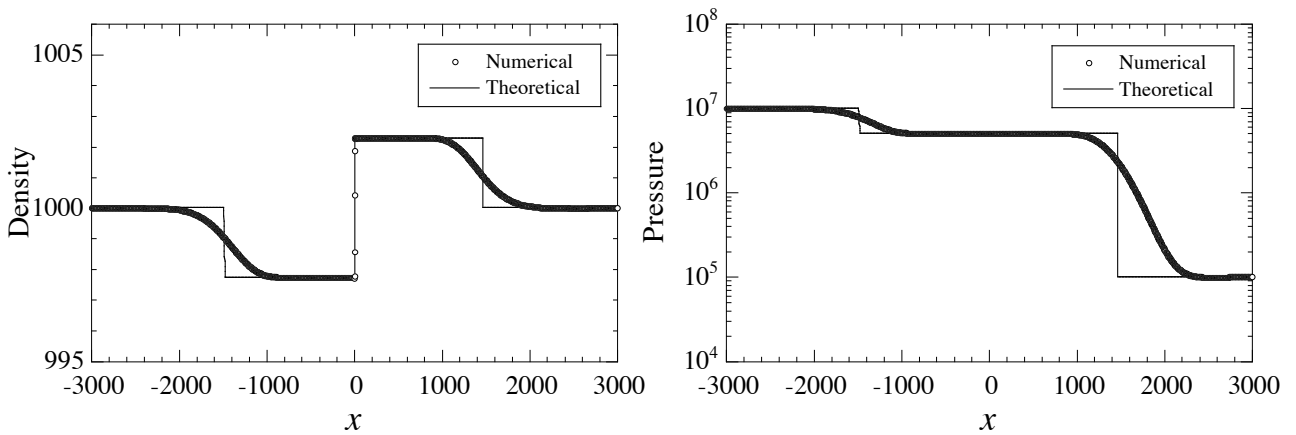


Fig.5.1.16 Results of case13 ( $p_R/p_L = 10^{-2}$ , SI, Tammann EOS)

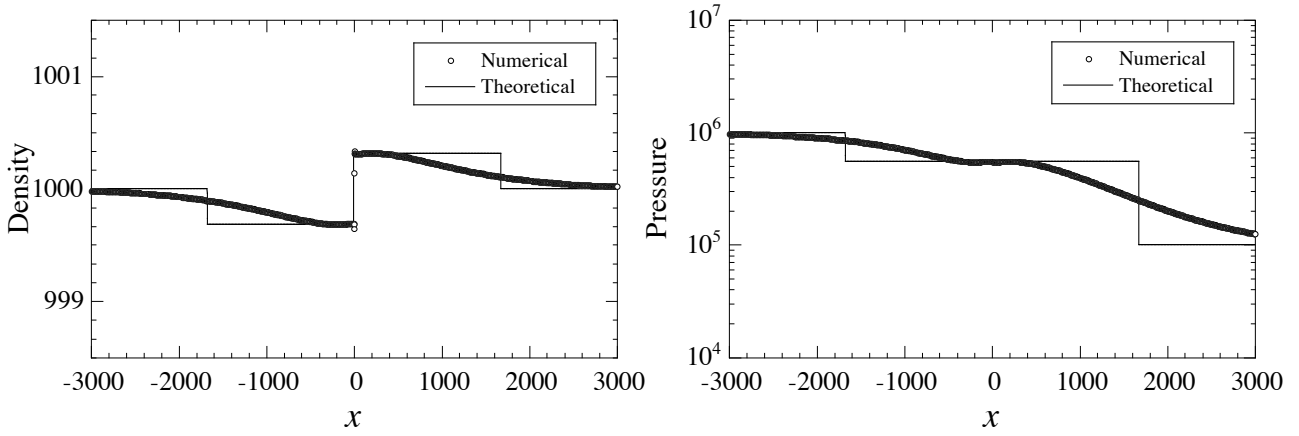


Fig. 5.1.17 Results of case14 ( $p_R/p_L = 10^{-1}$ , SI, Tammann EOS)

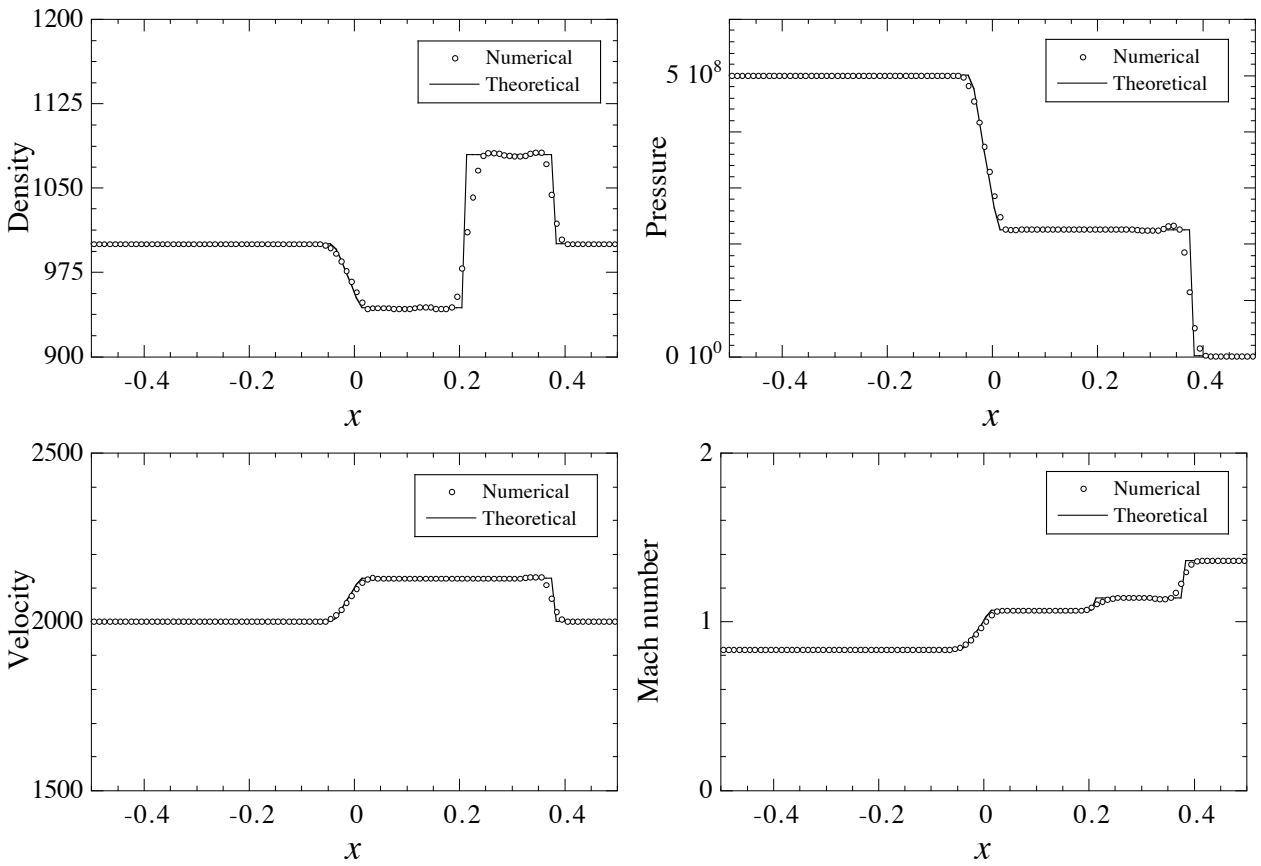


Fig.5.1.18 Results of case15 (Supersonic, EX, Tammann EOS)

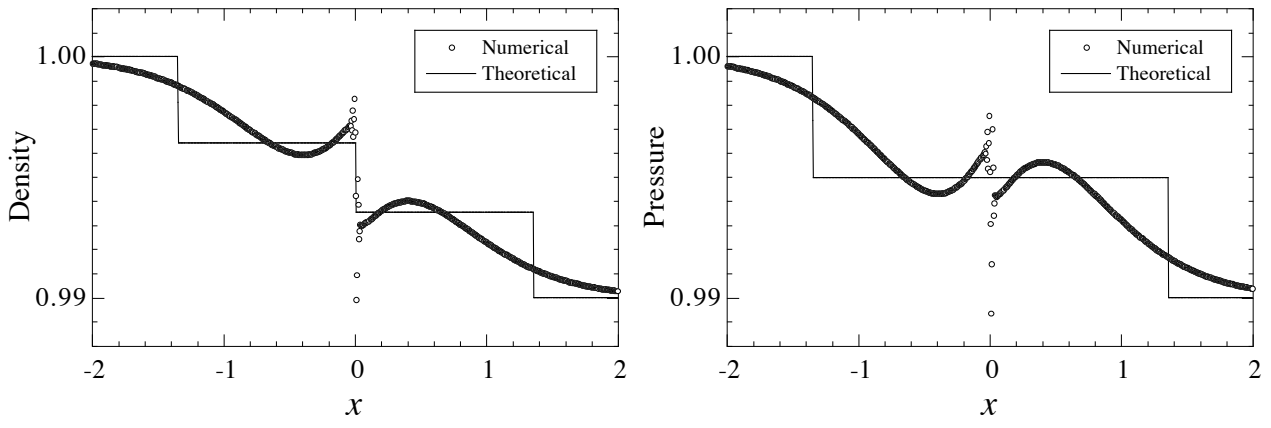


Fig. 5.1.19 Results of case9a (the GCUP *not used*,  $p_R/p_L = 0.999$ , SI, perfect gas)

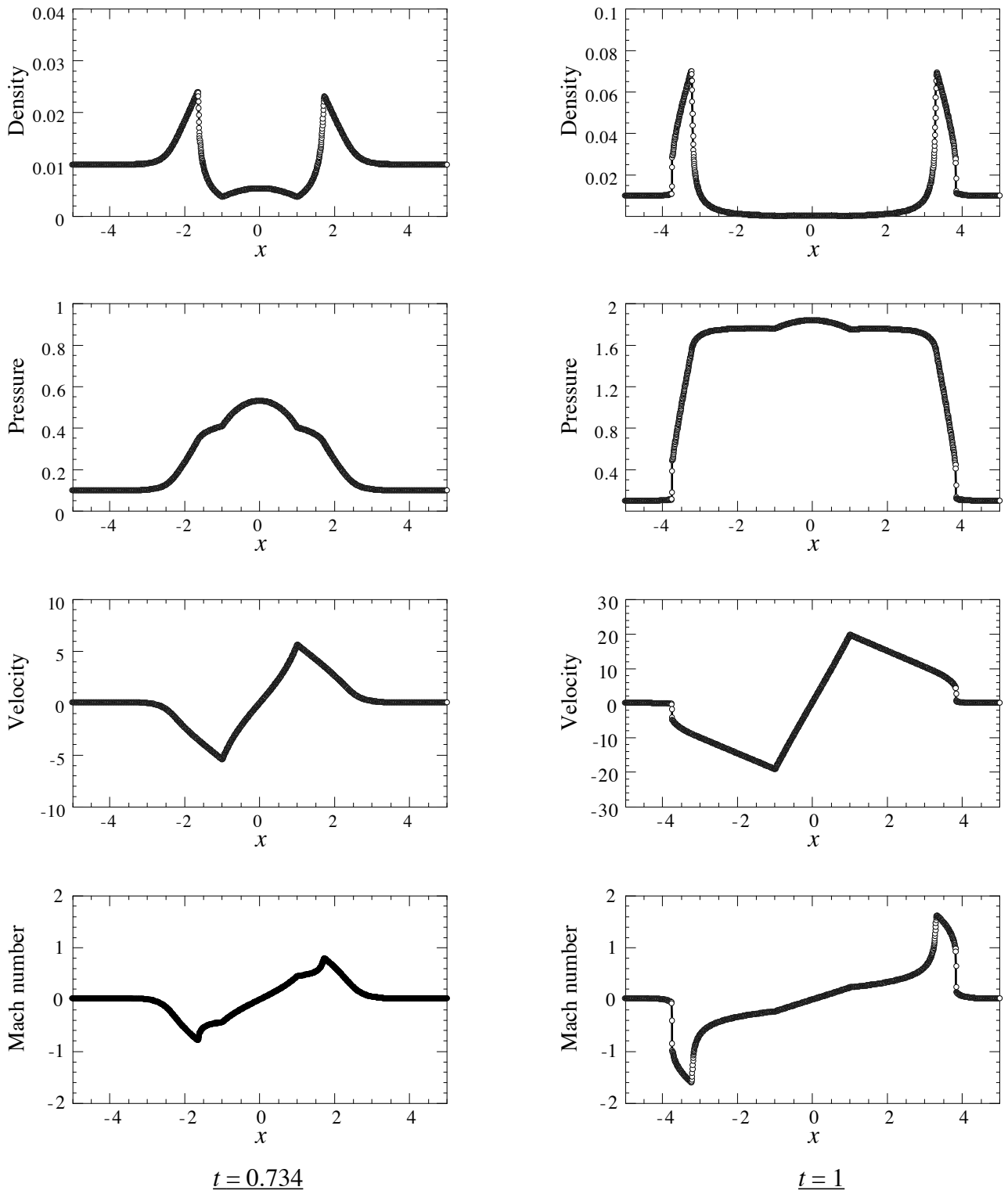


Fig.5.2.1 Results of flow transient case

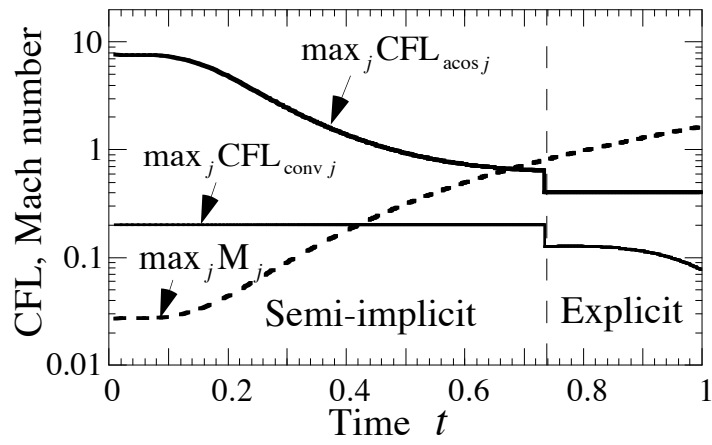


Fig.5.2.2 History of the Mach number and CFL numbers.

## Appendix Derivation of pressure equation, Eq.(12)

The pressure equation Eq.(12) which provides the prediction of  $p^{n+1}$  is derived as follows.

We start from the mass conservation equation in the vector form :

$$\partial \rho / \partial t + \text{div}(\rho \mathbf{u}) = 0. \quad (\text{A1})$$

Suppose isentropic process, we have  $dp/d\rho = c^2$  ( $c$  is the speed of sound), and substitute this into Eq.(A1) to yield

$$(1/c^2) \cdot \partial p / \partial t + \text{div}(\rho \mathbf{u}) = 0. \quad (\text{A2})$$

Taking the time derivative of Eq.(A2) with  $c$  frozen,

$$\partial^2 p / \partial t^2 + c^2 \text{div}(\partial \rho \mathbf{u} / \partial t) = 0. \quad (\text{A3})$$

From the momentum conservation equation,  $\partial \rho \mathbf{u} / \partial t = -\text{div}(\rho \mathbf{u} \otimes \mathbf{u}) - \text{grad} p$ , thus

$$\partial^2 p / \partial t^2 - c^2 \text{div grad} p = c^2 \text{div}(\text{div}(\rho \mathbf{u} \otimes \mathbf{u})). \quad (\text{A4})$$

It is noted that if we assume infinitesimal changes in the density and that the fluid almost remains stationary, Equation (A4) becomes the well-known linear wave equation,  $p_{tt} - c^2 \Delta p = 0$ .

We assign time level of discretization for each term of Eq.(A4) as :

$$\partial^2 p / \partial t^2 \Big|_j^n - (c_j^n)^2 \text{div grad} p^{n+1} \Big|_j = (c_j^n)^2 \text{div}(\text{div}(\rho \mathbf{u} \otimes \mathbf{u})^n) \Big|_j. \quad (\text{A5})$$

The first term can be discretized as :

$$\partial^2 p / \partial t^2 \Big|_j^n \approx (\partial p / \partial t \Big|_j^{n+1/2} - \partial p / \partial t \Big|_j^{n-1/2}) / \Delta t. \quad (\text{A6})$$

From  $dp/d\rho = c^2$  and a discretized form of Eq.(A1),

$$\partial p / \partial t \Big|_j^{n-1/2} \approx (c_j^n)^2 \partial \rho / \partial t \Big|_j^{n-1/2} \approx -(c_j^n)^2 \text{div}(\rho \mathbf{u})^n \Big|_j. \quad (\text{A7})$$

Rearrangement of Eqs.(A5)-(A7) leads to

$$\partial p / \partial t \Big|_j^{n+1/2} - \Delta t (c_j^n)^2 \text{div grad} p^{n+1} \Big|_j = -(c_j^n)^2 \text{div}((\rho \mathbf{u})^n - \Delta t \text{div}(\rho \mathbf{u} \otimes \mathbf{u})^n) \Big|_j. \quad (\text{A8})$$

Here, recall that the advanced momentum  $(\rho \mathbf{u})^{\text{ad}}$  has been defined in §4.2 as an explicit solution of the discretized momentum convection equation,  $\partial_t \rho \mathbf{u} + \text{div}(\rho \mathbf{u} \otimes \mathbf{u}) = 0$ . Then, we can put

$$(\rho \mathbf{u})^n - \Delta t \text{div}(\rho \mathbf{u} \otimes \mathbf{u})^n \approx (\rho \mathbf{u})^{\text{ad}}. \quad (\text{A9})$$

The term  $\partial p / \partial t \Big|_j^{n+1/2}$  in Eq.(A8) can be discretized as :

$$\partial p / \partial t \Big|_j^{n+1/2} \approx (p_j^{n+1} - p_j^n) / \Delta t. \quad (\text{A10})$$

Substituting Eq.(A9) and (A10) into (A8), we obtain the vector form of Eq.(12) :

$$(p_j^{n+1} - p_j^n) / \Delta t = \Delta t (c_j^n)^2 \text{div grad} p^{n+1} \Big|_j - (c_j^n)^2 \text{div}((\rho \mathbf{u})^{\text{ad}}) \Big|_j. \quad \square$$